Optimized Schwarz methods for the time-dependent Stokes–Darcy coupling

IMA Journal of Numerical Analysis (2023) **00**, 1–26
https://doi.org/10.1093/imanum/drad057

Optimized Schwarz methods for the time-dependent Stokes–Darcy coupling

Marco Discacciati*
Department of Mathematical Sciences, Loughborough University, Loughborough LE11 3TU, UK
*Corresponding author: m.discacciati@lboro.ac.uk

and

Tommaso Vanzan
Département de Mathématiques, École Polytechnique Fédérale de Lausanne, CH-1015 Lausanne, Switzerland
tommaso.vanzan@epfl.ch

[Received on 22 August 2022; revised on 24 February 2023]

This paper derives optimized coefficients for optimized Schwarz iterations for the time-dependent Stokes–Darcy problem using an innovative strategy to solve a nonstandard min-max problem. The coefficients take into account both physical and discretization parameters that characterize the coupled problem, and they guarantee the robustness of the associated domain decomposition method. Numerical results validate the proposed approach in several test cases with physically relevant parameters.

Keywords: Time-dependent Stokes–Darcy problem; Domain decomposition methods; Optimized Schwarz methods; Robin interface conditions.

1. Introduction

The Stokes–Darcy problem has been extensively studied during the last two decades due to its relevance to model filtration phenomena in industrial and natural applications. The steady problem introduced in the seminal works (Lagarias *et al.*, 1998; Discacciati *et al.*, 2002) has been extended to consider the time-dependent case in, e.g., Discacciati (2004b); Cao *et al.* (2010); Moraiti (2012); Çeşmelioğlu *et al.* (2013); Cao *et al.* (2014); Rybak & Magiera (2014).

In both settings, the spatial discretization of the Stokes–Darcy model leads to a large linear system (possibly at each time step) that has to be effectively preconditioned. A possible strategy to achieve this is to adopt a monolithic approach considering the whole coupled linear system at once (see, e.g., the recently proposed robust monolithic preconditioner derived using an operator preconditioning framework in Mardal & Winther, 2011). However, the multi-physics nature of the Stokes–Darcy problem makes it suitable for decoupled strategies based on domain decomposition that set up an iterative process where the Stokes and Darcy problems are solved separately at each iteration until convergence. Nevertheless, the computational efficiency of a domain decomposition approach depends on the number of subdomain iterations that are needed to reach convergence, especially in the time-dependent case. It is now well understood that the way in which the subdomain are coupled at each iteration significantly affects the convergence rate.

Earlier works focused on Dirichlet–Neumann algorithms (Discacciati & Quarteroni, 2004; Discacciati, 2004a; Discacciati & Quarteroni, 2009), FETI and BDD methods (Galvis & Sarkis, 2007, 2010), which however exhibit slow convergence for small values of the viscosity of the fluid and the permeability of the porous medium.

More recent efforts have focused on Robin–Robin transmission conditions (Discacciati *et al.*, 2007; Cao *et al.*, 2011; Chen *et al.*, 2011; Caiazzo *et al.*, 2014; He *et al.*, 2015), which generally show better properties in terms of convergence and robustness with respect to the physical parameters, provided that the Robin parameters are properly selected. Their optimization is usually carried out in a simplified geometrical setting using Fourier analysis. Robin-Robin domain decomposition methods that use optimized Robin parameters belong to the family of optimized Schwarz methods (Gander, 2006), which have been proven to be very effective, beyond the limitations set by the Fourier analysis, for several different equations (Dolean *et al.*, 2009; Gander & Xu, 2016; Gander & Vanzan, 2019, 2020b) and geometric configurations (Gigante & Vergara, 2016; Gigante *et al.*, 2020; Chen *et al.*, 2021). Optimized Schwarz methods have been first studied for the stationary Stokes–Darcy system in Discacciati & Gerardo-Giorda (2018) and Gander & Zhang (2019); Gander & Vanzan (2020a).

Few works have considered the time-dependent Stokes–Darcy coupling with Robin interface conditions. References Feng *et al.* (2012); Cao *et al.* (2014) present a loosely coupled implicit time-marching scheme that at each time step solves the Stokes and Darcy problems separately, without iterating. The two subdomains are coupled through a Robin boundary condition that depends on the solution computed in the other subdomain at the previous time step. Despite being noniterative and preserving optimal accuracy, this approach has the downside that the iterates do not fulfill the physical coupling conditions at each time step. Time parallel strategies based on waveform relaxation algorithms have instead been analyzed in Thi-Thao-Phuong *et al.* (2022).

In this work, we propose a novel approach where we perform a classical semi-discretization in time using a general implicit θ-method (Hairer *et al.*, 2002), and we optimize the convergence rate of a nonoverlapping Schwarz method to solve the local subproblems at each time step. For the optimization of the Schwarz method, we rely on Fourier analysis to derive the convergence factor of the iterative domain decomposition method in the frequency domain, and we study a min-max problem to characterize the optimized Robin parameters. Since the min-max problem differs from others in the existing literature, we develop a new theoretical argument that can be applied to min-max problems sharing the same structure. Numerical results performed with physically relevant parameters show that the optimized Schwarz method is robust and requires very few iterations to convergence at each time step, so that the method we propose is a valid alternative to noniterative time-marching schemes.

The rest of the manuscript is organized as follows. Section 2 formulates the problem, describes the semi-discretization in time and introduces the optimized Schwarz method. Section 3 performs a Fourier analysis and derives the optimized parameters by solving the min-max problem. Section 4 presents extensive numerical tests to assess the performance of the proposed algorithm.

2. Setting and formulation of the optimized Schwarz method

Let $\Omega \subset \mathbb{R}^{\mathrm{D}}$ ($\mathrm{D} = 2, 3$) be an open bounded domain formed by a fluid region Ω_f and a porous-medium region Ω_p with Lipschitz continuous boundaries $\partial\Omega_f$ and $\partial\Omega_p$. The two regions are nonoverlapping and separated by an interface Γ, i.e., $\overline{\Omega} = \overline{\Omega}_f \cup \overline{\Omega}_p$, $\Omega_f \cap \Omega_p = \emptyset$ and $\overline{\Omega}_f \cap \overline{\Omega}_p = \Gamma$, as illustrated in Fig. 1. Let $\mathbf{n}_p$ and $\mathbf{n}_f$ be the unit normal vectors pointing outwards of $\partial\Omega_p$ and $\partial\Omega_f$, respectively, with $\mathbf{n}_f = -\mathbf{n}_p$ on Γ. We assume that $\mathbf{n}_f$ and $\mathbf{n}_p$ are regular enough, and we indicate $\mathbf{n} = \mathbf{n}_f$ for simplicity.

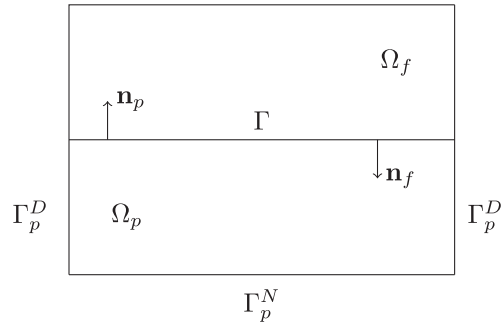

FIG. 1. Schematic representation of a 2D section of the computational domain.

In Ω_f and for time $t \in (0, T]$, we consider an incompressible fluid with constant viscosity and density described by the dimensionless time-dependent Stokes equations,

$$\partial_t \mathbf{u}_f - \nabla \cdot \left(2\mu_f \nabla^{\mathrm{s}} \mathbf{u}_f - p_f \boldsymbol{I}\right) = \mathbf{f}_f \qquad \text{in } \Omega_f, \tag{2.1a}$$

$$\nabla \cdot \mathbf{u}_f = 0 \qquad \text{in } \Omega_f, \tag{2.1b}$$

where $\mu_f = Re^{-1}$, Re being the Reynolds number, $\mathbf{u}_f$ and p_f are the fluid velocity and pressure, $\boldsymbol{I}$ and $\nabla^{\mathrm{s}} \mathbf{u}_f = \frac{1}{2}(\nabla \mathbf{u}_f + (\nabla \mathbf{u}_f)^T)$ are the identity and the strain rate tensor, and $\mathbf{f}_f$ is an external force. In the porous medium domain Ω_p and for $t \in (0, T]$, we consider the dimensionless time-dependent Darcy model (see, e.g., Cao *et al.*, 2010; Moraiti, 2012; Rybak & Magiera, 2014):

$$S_p \, \partial_t p_p - \nabla \cdot (\boldsymbol{\eta}_p \nabla p_p) = f_p \qquad \text{in } \Omega_p, \tag{2.2}$$

where p_p is the fluid pressure in the porous medium, $\boldsymbol{\eta}_p$ is the permeability tensor, S_p is the specific mass storativity coefficient, and f_p is an external force.

The two models are coupled through the classical Beavers–Joseph–Saffman conditions, which describe the filtration across the interface Γ (Beavers & Joseph, 1967; Saffman, 1971; Jäger & Mikelić, 1996; Rybak & Magiera, 2014):

$$\mathbf{u}_f \cdot \mathbf{n} = -(\boldsymbol{\eta}_p \nabla p_p) \cdot \mathbf{n} \qquad \text{at } \Gamma, \tag{2.3a}$$

$$-\mathbf{n} \cdot \left(2\mu_f \nabla^{\mathrm{s}} \mathbf{u}_f - p_f \boldsymbol{I}\right) \cdot \mathbf{n} = p_p \qquad \text{at } \Gamma, \tag{2.3b}$$

$$-\left(\left(2\mu_f \nabla^{\mathrm{s}} \mathbf{u}_f - p_f \boldsymbol{I}\right) \cdot \mathbf{n}\right)_\tau = \xi_f (\mathbf{u}_f)_\tau \qquad \text{at } \Gamma, \tag{2.3c}$$

where $\xi_f = \alpha_{BJ} \mu_f / \sqrt{\boldsymbol{\tau} \cdot \boldsymbol{\eta}_p \cdot \boldsymbol{\tau}}$ and α_{BJ} is a dimensionless constant which depends on the geometric structure of the porous medium. The notation $(\mathbf{v})_\tau$ indicates the tangential component of any vector $\mathbf{v}$ at Γ, i.e., $(\mathbf{v})_\tau = \mathbf{v} - (\mathbf{v} \cdot \mathbf{n})\,\mathbf{n}$ at Γ. As boundary conditions, we impose $p_p = 0$ on Γ_p^D, $\mathbf{u}_p \cdot \mathbf{n}_p = 0$ on Γ_p^N, and $\mathbf{u}_f = \mathbf{0}$ on $\partial\Omega_f \setminus \Gamma$ as in Discacciati & Gerardo-Giorda (2018) (see Fig. 1 for the notation), and as

initial conditions we set

$$\mathbf{u}_f = \mathbf{u}_f^0 \quad \text{in } \Omega_f \quad \text{and} \quad p_p = p_p^0 \quad \text{in } \Omega_p \quad \text{at } t = 0, \tag{2.4}$$

with $\mathbf{u}_f^0$ and p_p^0 given functions.

We define the spaces

$$\mathbf{V}_f := \left\{ \mathbf{v} \in \mathbf{H}^1(\Omega_f) \,:\, \mathbf{v} = \mathbf{0} \quad \text{on } \partial\Omega_f \setminus \Gamma \right\}, \quad Q_f := L^2(\Omega_f),$$

$$Q_p := \left\{ q \in H^1(\Omega_p) \,:\, q = 0 \quad \text{on } \Gamma_p^D \right\},$$

and let $(\cdot,\cdot)_{\mathcal{D}}$ be the L^2 scalar product in a domain $\mathcal{D}$ for scalar, vector, or tensor functions, while $\langle\cdot,\cdot\rangle_\Gamma$ is the scalar product in $H^{1/2}(\Gamma)$. Then, we introduce the bilinear forms

$$a_f : \mathbf{V}_f \times \mathbf{V}_f \to \mathbb{R}, \quad a_f(\mathbf{v},\mathbf{w}) = \left(2\mu_f \nabla^{\mathrm{s}}\mathbf{v}, \nabla^{\mathrm{s}}\mathbf{w}\right)_{\Omega_f} + \xi_f \langle (\mathbf{v})_\tau, (\mathbf{w})_\tau \rangle_\Gamma,$$

$$b_f : \mathbf{V}_f \times Q_f \to \mathbb{R}, \quad b_f(\mathbf{v}, q) = -(\nabla \cdot \mathbf{v}, q)_{\Omega_f},$$

$$a_p : Q_p \times Q_p \to \mathbb{R}, \quad a_p(p,q) = \left(\boldsymbol{\eta}_p \nabla p, \nabla q\right)_{\Omega_p}.$$

The weak formulation of problem (2.1)–(2.3) can be written as follows: for all $t \in (0,T]$, find $\mathbf{u}_f(t) \in \mathbf{V}_f$, $p_f(t) \in Q_f$, and $p_p(t) \in Q_p$ such that

$$(\partial_t \mathbf{u}_f, \mathbf{v}_f)_{\Omega_f} + a_f(\mathbf{u}_f, \mathbf{v}_f) + b_f(\mathbf{v}_f, p_f) + \langle p_p, \mathbf{v}_f \cdot \mathbf{n}\rangle_\Gamma = (\mathbf{f}_f, \mathbf{v})_{\Omega_f} \qquad \forall \mathbf{v}_f \in \mathbf{V}_f, \tag{2.5a}$$

$$b_f(\mathbf{u}_f, q_f) = 0 \qquad \forall q_f \in Q_f, \tag{2.5b}$$

$$(S_p\, \partial_t p_p, q_p)_{\Omega_p} + a_p(p_p, q_p) - \langle \mathbf{u}_f \cdot \mathbf{n}, q_p\rangle_\Gamma = (f_p, q)_{\Omega_p} \qquad \forall q_p \in Q_p, \tag{2.5c}$$

with initial conditions (2.4). For all $t \in (0,T]$, the weak formulation (2.5) admits a unique solution $(\mathbf{u}_f(t), p_f(t), p_p(t)) \in \mathbf{V}_f \times Q_f \times Q_p$ which depends continuously on the data (see, e.g., Discacciati, 2004a). We remark that the scalar product $\langle\cdot,\cdot\rangle_\Gamma$ can be used both in (2.5) and in the definition of the bilinear form a_f due to the regularity assumption on $\mathbf{n}$ at Γ.

2.1 *Optimized Schwarz method*

To formulate the optimized Schwarz method for the time-dependent Stokes–Darcy problem, we introduce a linear combination of the interface conditions (2.3a) and (2.3b) with coefficients $(-\alpha_f, 1)$ and $(\alpha_p, 1)$, α_f, α_p being positive real parameters. This leads to the Robin transmission conditions

$$-\mathbf{n} \cdot \left(2\mu_f \nabla^{\mathrm{s}}\mathbf{u}_f - p_f \boldsymbol{I}\right) \cdot \mathbf{n} - \alpha_f \mathbf{u}_f \cdot \mathbf{n} = p_p + \alpha_f\, \boldsymbol{\eta}_p \nabla p_p \cdot \mathbf{n} \quad \text{at } \Gamma, \tag{2.6}$$

and

$$p_p - \alpha_p\, \boldsymbol{\eta}_p \nabla p_p \cdot \mathbf{n} = -\mathbf{n} \cdot \Big(2\mu_f \nabla^{\mathrm{s}} \mathbf{u}_f - p_f \boldsymbol{I}\Big) \cdot \mathbf{n} + \alpha_p \mathbf{u}_f \cdot \mathbf{n} \quad \text{at } \Gamma. \tag{2.7}$$

The coefficients α_f and α_p must be suitably chosen in order to optimize the convergence rate of the iterative algorithm that we formulate hereafter using the Robin–Robin transmission conditions (2.6) and (2.7).

Upon setting

$$\lambda_f(t) = p_p + \alpha_f\, \boldsymbol{\eta}_p \nabla p_p \cdot \mathbf{n} \quad \text{and} \quad \lambda_p(t) = -\mathbf{n} \cdot \Big(2\mu_f \nabla^{\mathrm{s}} \mathbf{u}_f - p_f \boldsymbol{I}\Big) \cdot \mathbf{n} + \alpha_p\, \mathbf{u}_f \cdot \mathbf{n},$$

the Robin interface conditions (2.6) and (2.7) can be used to equivalently reformulate problem (2.5) as follows: for all $t \in (0, T]$, find $\mathbf{u}_f(t) \in \mathbf{V}_f$, $p_f(t) \in Q_f$, and $p_p(t) \in Q_p$ such that

$$(\partial_t \mathbf{u}_f, \mathbf{v}_f)_{\Omega_f} + a_f(\mathbf{u}_f, \mathbf{v}_f) + b_f(\mathbf{v}_f, p_f) + \alpha_f \langle \mathbf{u}_f \cdot \mathbf{n}, \mathbf{v}_f \cdot \mathbf{n} \rangle_\Gamma = (\mathbf{f}_f, \mathbf{v})_{\Omega_f} - \langle \lambda_f, \mathbf{v}_f \cdot \mathbf{n} \rangle_\Gamma, \tag{2.8a}$$

$$b_f(\mathbf{u}_f, q_f) = 0, \tag{2.8b}$$

$$(S_p\, \partial_t p_p, q_p)_{\Omega_p} + a_p(p_p, q_p) + \frac{1}{\alpha_p} \langle p_p, q_p \rangle_\Gamma = (f_p, q)_{\Omega_p} + \frac{1}{\alpha_p} \langle \lambda_p, q_p \rangle_\Gamma, \tag{2.8c}$$

for all $\mathbf{v}_f \in \mathbf{V}_f$, $q_f \in Q_f$, and $q_p \in Q_p$.

For the time discretization of problem (2.8), we split the interval $[0, T]$ into equal subintervals $[t^{n-1}, t^n]$ such that $[0, T] = \cup_{n=1}^N [t^{n-1}, t^n]$, with $t^0 = 0$, $t^N = T$ and $\Delta t = t^n - t^{n-1}$, and we consider the θ-method (see, e.g., Turek, 1996; Hairer *et al.*, 2002; John *et al.*, 2006) with $\theta \in (0, 1]$. We are particularly interested in the cases $\theta = 1$ and $\theta = \frac{1}{2}$, which correspond to the implicit Euler method and to the Crank–Nicolson method.

For simplicity of notation, let us define the bilinear forms

$$\widetilde{a}_f : \mathbf{V}_f \times \mathbf{V}_f \to \mathbb{R}, \quad \widetilde{a}_f(\mathbf{v}, \mathbf{w}) = (\mathbf{v}, \mathbf{w})_{\Omega_f} + \theta\, \Delta t \left(a_f(\mathbf{v}, \mathbf{w}) + \alpha_f \langle \mathbf{v} \cdot \mathbf{n}, \mathbf{w} \cdot \mathbf{n} \rangle_\Gamma \right),$$

$$\widetilde{a}_p : Q_p \times Q_p \to \mathbb{R}, \quad \widetilde{a}_p(p, q) = (S_p\, p, q)_{\Omega_p} + \theta\, \Delta t \left(a_p(p, q) + \frac{1}{\alpha_p} \langle p, q \rangle_\Gamma \right),$$

and the functionals $F_f^n : \mathbf{V}_f \to \mathbb{R}$ and $F_p^n : Q_p \to \mathbb{R}$

$$\begin{aligned} F_f^n(\mathbf{v}) \;=\; & \Delta t \left(\theta \left(\mathbf{f}_f^n, \mathbf{v} \right)_{\Omega_f} + (1-\theta) \left(\mathbf{f}_f^{n-1}, \mathbf{v} \right)_{\Omega_f} \right) + \left(\mathbf{u}_f^{n-1}, \mathbf{v} \right)_{\Omega_f} \\ & - (1-\theta)\, \Delta t \left(a_f \left(\mathbf{u}_f^{n-1}, \mathbf{v} \right) + \alpha_f \left\langle \mathbf{u}_f^{n-1} \cdot \mathbf{n}, \mathbf{v} \cdot \mathbf{n} \right\rangle + \left\langle \lambda_f^{n-1}, \mathbf{v}_f \cdot \mathbf{n} \right\rangle \right), \\ F_p^n(q) \;=\; & \Delta t \left(\theta \left(f_p^n, q \right)_{\Omega_p} + (1-\theta) \left(f_p^{n-1}, q \right)_{\Omega_p} \right) + \left(S_p\, p_p^{n-1}, q \right)_{\Omega_p} \\ & - (1-\theta)\, \Delta t \left(a_p \left(p_p^{n-1}, q \right) + \tfrac{1}{\alpha_p} \left\langle p_p^{n-1}, q \right\rangle_\Gamma - \tfrac{1}{\alpha_p} \left\langle \lambda_p^{n-1}, q_p \right\rangle \right). \end{aligned}$$

Then, starting from the initial condition (2.4), for $n = 1, \dots, N$, we compute $(\mathbf{u}_f^n, p_f^n, p_p^n) \in \mathbf{V}_f \times Q_f \times Q_p$ solution of

$$\widetilde{a}\left(\mathbf{u}_f^n, \mathbf{v}_f^n\right) + \Delta t\, b_f\left(\mathbf{v}_f, p_f^n\right) = F_f^n(\mathbf{v}_f) - \theta\, \Delta t \left\langle \lambda_f^n, \mathbf{v}_f \cdot \mathbf{n} \right\rangle_\Gamma \qquad \forall \mathbf{v}_f \in V_f, \tag{2.9a}$$

$$b_f\left(\mathbf{u}_f^n, q_f\right) = 0 \qquad \forall q_f \in Q_f, \tag{2.9b}$$

$$\widetilde{a}_p\left(p_p^n, q_p\right) = F_p^n(q_p) + \frac{\theta\, \Delta t}{\alpha_p} \left\langle \lambda_p^n, q_p \right\rangle_\Gamma \qquad \forall q_p \in Q_p, \tag{2.9c}$$

where

$$\lambda_f^n = p_p^n + \alpha_f\, \boldsymbol{\eta}_p \nabla p_p^n \cdot \mathbf{n}, \qquad \lambda_p^n = -\mathbf{n} \cdot \left(2\mu_f \nabla^{\mathrm{s}} \mathbf{u}_f^n - p_f^n \boldsymbol{I}\right) \cdot \mathbf{n} + \alpha_p\, \mathbf{u}_f^n \cdot \mathbf{n}.$$

At each time level $n \geq 1$, system (2.9) is still fully coupled. To decouple the Stokes and the Darcy equations, we consider the optimized Schwarz iterative scheme, which starts from the initial guess $\lambda_f^{n,0}$, and, for $m \geq 1$ until convergence, it computes

$$\widetilde{a}\left(\mathbf{u}_f^{n,m}, \mathbf{v}_f^n\right) + \Delta t\, b_f\left(\mathbf{v}_f, p_f^{n,m}\right) = F_f^n(\mathbf{v}_f) - \theta\, \Delta t \left\langle \lambda_f^{n,m-1}, \mathbf{v}_f \cdot \mathbf{n} \right\rangle_\Gamma \qquad \forall \mathbf{v}_f \in V_f, \tag{2.10a}$$

$$b_f\left(\mathbf{u}_f^{n,m}, q_f\right) = 0 \qquad \forall q_f \in Q_f, \tag{2.10b}$$

$$\widetilde{a}_p\left(p_p^{n,m}, q_p\right) = F_p^n(q_p) + \frac{\theta\, \Delta t}{\alpha_p} \left\langle \lambda_p^{n,m}, q_p \right\rangle_\Gamma \qquad \forall q_p \in Q_p, \tag{2.10c}$$

where

$$\lambda_f^{n,m} = p_p^{n,m} + \alpha_f\, \boldsymbol{\eta}_p \nabla p_p^{n,m} \cdot \mathbf{n}, \quad \lambda_p^{n,m} = -\mathbf{n} \cdot \left(2\mu_f \nabla^{\mathrm{s}} \mathbf{u}_f^{n,m} - p_f^{n,m} \boldsymbol{I}\right) \cdot \mathbf{n} + \alpha_p\, \mathbf{u}_f^{n,m} \cdot \mathbf{n}.$$

Standard calculations (see, e.g., Discacciati & Gerardo-Giorda, 2018; Gander & Vanzan, 2020a) show that, for an initial guess $\lambda_p^{n,0}$ and $m \geq 1$,

$$\lambda_f^{n,m} = \left(1 + \frac{\alpha_f}{\alpha_p}\right) p_p^{n,m} - \frac{\alpha_f}{\alpha_p} \lambda_p^{n,m-1}, \tag{2.11a}$$

$$\lambda_p^{n,m} = (\alpha_f + \alpha_p)\, \mathbf{u}_f^{n,m} \cdot \mathbf{n} + \lambda_f^{n,m}. \tag{2.11b}$$

Notice that a parallel version of the optimized Schwarz scheme can be obtained by taking $\lambda_p^{n,m-1}$ in (2.10c) and $\lambda_f^{n,m-1}$ in (2.11b).

We conclude this section by showing that the iteration scheme (2.10) can be reformulated only in terms of the interface functions $\lambda_f^{n,m}$ and $\lambda_p^{n,m}$ at Γ. To this aim, in the domain Ω_f, we define the

continuous trace operator $\tau_f : \mathbf{V}_f \times Q_f \to H^{\frac{1}{2}}(\Gamma)$ as $\tau_f((\mathbf{v},p)) = (\mathbf{v}\cdot\mathbf{n})_{|\Gamma}$, and the continuous extension operator $\mathcal{E}_f : H^{-\frac{1}{2}}(\Gamma) \times \mathbf{V}_f^{-1} \to \mathbf{V}_f \times Q_f$ as $\mathcal{E}_f(\lambda, \mathcal{F}_f) = (\mathbf{v},p)$, where $(\mathbf{v},p)$ is the solution of

$$\begin{aligned} \widetilde{a}_f(\mathbf{v},\mathbf{w}) + \Delta t\, b_f(\mathbf{v},p) &= \mathcal{F}_f(\mathbf{w}) - \theta\, \Delta t \,\langle \lambda, \mathbf{w}\cdot\mathbf{n}\rangle_\Gamma \qquad \forall \mathbf{w} \in \mathbf{V}_f, \\ b_f(\mathbf{v},q) &= 0 \qquad \forall q \in Q_f. \end{aligned}$$

Similarly in the domain Ω_p, we define the continuous trace operator $\tau_p : Q_p \to H^{\frac{1}{2}}(\Gamma)$ as $\tau_p(q) = q_{|\Gamma}$, and the continuous extension operator $\mathcal{E}_p : H^{-\frac{1}{2}}(\Gamma) \times Q_p^{-1} \to Q_p$ as $\mathcal{E}_p(\lambda, \mathcal{F}_p) = p$, where p is the solution of

$$\widetilde{a}_p(p,q) = \mathcal{F}_p(q) + \frac{\theta\, \Delta t}{\alpha_p}\langle \lambda, q\rangle \qquad \forall q \in Q_p.$$

Then, relations (2.11) can be equivalently reformulated as

$$\lambda_f^{n,m} = \left(1 + \frac{\alpha_f}{\alpha_p}\right) \tau_p\left(\mathcal{E}_p\left(\lambda_p^{n,m-1}, F_p^n\right)\right) - \frac{\alpha_f}{\alpha_p}\lambda_p^{n,m-1}, \tag{2.12a}$$

$$\lambda_p^{n,m} = (\alpha_f + \alpha_p)\, \tau_f\left(\mathcal{E}_f\left(\lambda_f^{n,m}, F_f^n\right)\right) + \lambda_f^{n,m}. \tag{2.12b}$$

Now define the linear continuous operators

$$\begin{aligned} &\mathcal{G}_f : H^{-\frac{1}{2}}(\Gamma) \to H^{\frac{1}{2}}(\Gamma), \qquad \mathcal{G}_f(\lambda) := \tau_f\left(\mathcal{E}_f(\lambda, 0)\right), \\ &\mathcal{G}_p : H^{-\frac{1}{2}}(\Gamma) \to H^{\frac{1}{2}}(\Gamma), \qquad \mathcal{G}_p(\lambda) := \tau_p\left(\mathcal{E}_p(\lambda, 0)\right). \end{aligned}$$

Thanks to the linearity of the extension operators $\mathcal{E}_f$ and $\mathcal{E}_p$, and setting

$$\chi_f^n = \left(1 + \frac{\alpha_f}{\alpha_p}\right)\tau_p(\mathcal{E}_p(0, F_p^n)), \qquad \chi_p^n = (\alpha_f + \alpha_p)\, \tau_f\left(\mathcal{E}_f\left(0, F_f^n\right)\right),$$

equation (2.12) can be equivalently written as

$$\begin{pmatrix} \lambda_f^{n,m} \\ \lambda_p^{n,m} \end{pmatrix} = \begin{pmatrix} 0 & -\frac{\alpha_f}{\alpha_p} I + \left(1 + \frac{\alpha_f}{\alpha_p}\right) \mathcal{G}_p(\cdot) \\ (\alpha_f + \alpha_p)\, \mathcal{G}_f(\cdot) + I & 0 \end{pmatrix} \begin{pmatrix} \lambda_f^{n,m-1} \\ \lambda_p^{n,m} \end{pmatrix} + \begin{pmatrix} \chi_f^n \\ \chi_p^n \end{pmatrix}. \tag{2.13}$$

This corresponds to a Gauss–Seidel step for the linear interface system

$$\begin{pmatrix} I & \frac{\alpha_f}{\alpha_p} I - \left(1 + \frac{\alpha_f}{\alpha_p}\right) \mathcal{G}_p(\cdot) \\ -(\alpha_f + \alpha_p)\, \mathcal{G}_f(\cdot) - I & I \end{pmatrix} \begin{pmatrix} \lambda_f^n \\ \lambda_p^n \end{pmatrix} = \begin{pmatrix} \chi_f^n \\ \chi_p^n \end{pmatrix}, \tag{2.14}$$

which can be more effectively solved using a suitable Krylov method (e.g., GMRES, Saad & Schultz, 1986) as we will do in Section 4. Notice that a sufficient condition for (2.14) to be solvable is that the stationary iteration (2.13) converges.

3. Analysis of the optimized Schwarz method

In this section, we analyse the optimized Schwarz method (2.10) with the aim of characterizing values of the parameters α_f and α_p to accelerate the convergence of the method. The expression of the convergence rate is obtained in Section 3.1, while the optimization of the parameters is carried out in Section 3.2 under the simplifying hypothesis that the Beavers–Joseph–Saffman interface condition (2.3c) is replaced by the zero tangential velocity condition $(\mathbf{u}_f)_\tau = 0$ at Γ. For the sake of simplicity, we restrict to a two-dimensional domain Ω. The three-dimensional case can be analyzed with the same methodology, but at the cost of more tedious calculations.

3.1 *Characterization of the convergence rate*

Since the problem is linear, for the analysis of the optimized Schwarz method (2.10) we directly consider the error equation obtained by setting $\mathbf{f}_f = \mathbf{0}$ and $f_p = 0$. More precisely, at time step $n \geq 1$, for $m \geq 1$ until convergence, we consider

1. the Stokes problem: find $\mathbf{u}_f^{n,m}, p_f^{n,m}$ such that

$$\frac{\mathbf{u}_f^{n,m}}{\Delta t} - \theta\, \nabla \cdot \left(2\mu_f\, \nabla^{\mathrm{s}} \mathbf{u}_f^{n,m}\right) + \nabla p_f^{n,m} = \mathbf{0} \qquad \text{in } \Omega_f, \tag{3.1a}$$

$$\nabla \cdot \mathbf{u}_f^{n,m} = 0 \qquad \text{in } \Omega_f, \tag{3.1b}$$

$$-\left(\left(2\mu_f \nabla^{\mathrm{s}} \mathbf{u}_f^{n,m} - p_f^{n,m} \boldsymbol{I}\right) \cdot \mathbf{n}\right)_\tau = \xi_f \left(\mathbf{u}_f^{n,m}\right)_\tau \qquad \text{at } \Gamma, \tag{3.1c}$$

$$-\mathbf{n} \cdot \left(2\mu_f \nabla^{\mathrm{s}} \mathbf{u}_f^{n,m} - p_f^{n,m} \boldsymbol{I}\right) \cdot \mathbf{n} - \alpha_f \mathbf{u}_f^{n,m} \cdot \mathbf{n} = p_p^{n,m-1} + \alpha_f\, \boldsymbol{\eta}_p \nabla p_p^{n,m-1} \cdot \mathbf{n} \qquad \text{at } \Gamma, \tag{3.1d}$$

2. the Darcy problem: find $p_p^{n,m}$ such that

$$\frac{S_p}{\Delta t}\, p_p^{n,m} - \theta\, \nabla \cdot \left(\boldsymbol{\eta}_p \nabla p_p^{n,m}\right) = 0 \qquad \text{in } \Omega_p, \tag{3.2a}$$

$$p_p^{n,m} - \alpha_p\, \boldsymbol{\eta}_p \nabla p_p^{n,m} \cdot \mathbf{n} = -\mathbf{n} \cdot \left(2\mu_f \nabla^{\mathrm{s}} \mathbf{u}_f^{n,m} - p_f^{n,m} \boldsymbol{I}\right) \cdot \mathbf{n} + \alpha_p\, \mathbf{u}_f^{n,m} \cdot \mathbf{n} \qquad \text{at } \Gamma. \tag{3.2b}$$

We introduce the setting considered, e.g., in Section 3.2 of Discacciati & Gerardo-Giorda (2018). Let Ω_f be the half plane $\Omega_f = \{(x,y) \in \mathbb{R}^2 \,:\, x < 0\}$, Ω_p be the complementary half plane $\Omega_p = \{(x,y) \in \mathbb{R}^2 \,:\, x > 0\}$, and $\Gamma = \{(x,y) \in \mathbb{R}^2 \,:\, x = 0\}$, so that $\mathbf{n} = (1,0)$, $\boldsymbol{\tau} = (0,1)$. Finally, let μ_f be constant in Ω_f, $\boldsymbol{\eta}_p = \mathrm{diag}(\eta_1, \eta_2)$ with η_1 and η_2 constant, and let $\mathbf{u}_f(x,y) = (u_1(x,y), u_2(x,y))^T$.

Using this setting and omitting the upper index n for simplicity of notation, the algorithm (3.1)–(3.2) becomes: for $m \geq 1$ until convergence, solve

1. the Stokes problem

$$\frac{1}{\Delta t}\begin{pmatrix} u_1^m \\ u_2^m \end{pmatrix} - \theta\,\mu_f \begin{pmatrix} \left(\partial_{xx}+\partial_{yy}\right) u_1^m \\ \left(\partial_{xx}+\partial_{yy}\right) u_2^m \end{pmatrix} + \begin{pmatrix} \partial_x p_f^m \\ \partial_y p_f^m \end{pmatrix} = \mathbf{0} \qquad \text{in } (-\infty,0)\times\mathbb{R}, \tag{3.3a}$$

$$\partial_x u_1^m + \partial_y u_2^m = 0 \qquad \text{in } (-\infty,0)\times\mathbb{R}, \tag{3.3b}$$

$$-\mu_f(\partial_x u_2 + \partial_y u_1) = \xi_f\, u_2^m \qquad \text{at } \{0\}\times\mathbb{R}, \tag{3.3c}$$

$$\left(-2\mu_f\,\partial_x u_1^m + p_f^m\right) - \alpha_f\, u_1^m = p_p^{m-1} - \alpha_f\left(-\eta_1\,\partial_x p_p^{m-1}\right) \qquad \text{at } \{0\}\times\mathbb{R}; \tag{3.3d}$$

2. the Darcy problem

$$\frac{S_p}{\Delta t}\,p_p^m - \theta\,(\partial_x(\eta_1\,\partial_x) + \partial_y(\eta_2\,\partial_y))\,p_p^m = 0 \qquad \text{in } (0,\infty)\times\mathbb{R}, \tag{3.4a}$$

$$p_p^m + \alpha_p\left(-\eta_1\,\partial_x p_p^m\right) = \left(-2\mu_f\,\partial_x u_1^m + p_f^m\right) + \alpha_p\,u_1^m \qquad \text{at } \{0\}\times\mathbb{R}. \tag{3.4b}$$

For the convergence analysis, similarly to Discacciati & Gerardo-Giorda (2018), we apply the Fourier transform in the direction tangential to the interface. In this case, for $w(x,y) \in L^2(\mathbb{R}^2)$, the Fourier transform is defined as

$$w(x,y) \mapsto \widehat{w}(x,k) = \int_{\mathbb{R}} e^{-iky}\, w(x,y)\,\mathrm{d}y,$$

where $k \in \mathbb{R}$ is the frequency variable.

The following results holds.

Proposition 3.1 The convergence factor of the iterative method (3.3a)–(3.4b) does not depend on the iteration m and it can be characterized for every $k \neq 0$ as $|\rho(k,\alpha_f,\alpha_p)|$ with

$$\rho(k,\alpha_f,\alpha_p) = \frac{\mathcal{G}(k)-\alpha_f}{\mathcal{G}(k)+\alpha_p}\cdot\frac{\mathcal{H}(k)-\alpha_p}{\mathcal{H}(k)+\alpha_f}, \tag{3.5}$$

where

$$\mathcal{G}(k) = \eta_p^{-1}\left(k^2 + \frac{S_p}{\eta_2\,\theta\,\Delta t}\right)^{-\frac{1}{2}}, \tag{3.6}$$

$$\mathcal{H}(k) = \frac{2\mu_f\left(k^2 + \frac{1}{\mu_f\,\theta\,\Delta t}\right)^{\frac{1}{2}} - \left(2\mu_f k^2\,\Delta t + 1\right)\mathcal{F}(k)}{1 - |k|\,\Delta t\,\mathcal{F}(k)}, \tag{3.7}$$

and

$$\mathcal{F}(k) = \frac{\mu_f k^2 + \left(\mu_f \left(k^2 + \frac{1}{\mu_f\,\theta\,\Delta t}\right)^{\frac{1}{2}} + \xi_f\right)\left(k^2 + \frac{1}{\mu_f\,\theta\,\Delta t}\right)^{\frac{1}{2}}}{k^2 \Delta t\,(2\mu_f|k| + \xi_f)}, \tag{3.8}$$

where $\eta_p = \sqrt{\eta_1 \eta_2}$.

Proof. Following analogous steps as in the proof of Proposition 3.1 of Discacciati & Gerardo-Giorda (2018), the Stokes pressure in the frequency space can be written as

$$\hat{p}_f^m(x,k) = P^m(k)\, e^{\,|k|x}. \tag{3.9}$$

The Fourier transform of the first component of the Stokes momentum equation (3.3a) becomes

$$\frac{\hat{u}_1^m}{\Delta t} - \theta\,\mu_f \partial_{xx}\hat{u}_1^m + \theta\,\mu_f k^2 \hat{u}_1^m + \partial_x \hat{p}_f^m = 0,$$

or, equivalently,

$$\partial_{xx}\hat{u}_1^m - \left(k^2 + \frac{1}{\mu_f\,\theta\,\Delta t}\right)\hat{u}_1^m = \frac{|k|}{\mu_f\,\theta} P^m(k)\, e^{\,|k|x}.$$

The general solution of this equation is

$$\hat{u}_1^m(x,k) = A^m(k)\, e^{\left(k^2 + \frac{1}{\mu_f\,\theta\,\Delta t}\right)^{1/2} x} - |k|\,\Delta t\, P^m(k)\, e^{|k|x}. \tag{3.10}$$

The Fourier transform of the second component of the Stokes momentum equation (3.3a) becomes

$$\frac{\hat{u}_2^m}{\Delta t} - \theta\,\mu_f \partial_{xx}\hat{u}_2^m + \theta\,\mu_f k^2 \hat{u}_2^m + ik\,\hat{p}_f^m = 0,$$

or, equivalently,

$$\partial_{xx}\hat{u}_2^m - \left(k^2 + \frac{1}{\mu_f\,\theta\,\Delta t}\right)\hat{u}_2^m = \frac{ik}{\mu_f\,\theta} P^m(k)\, e^{\,|k|x}.$$

The general solution of this equation is

$$\hat{u}_2^m(x,k) = B^m(k)\, e^{\left(k^2 + \frac{1}{\mu_f\,\theta\,\Delta t}\right)^{1/2} x} - ik\,\Delta t\, P^m(k)\, e^{|k|x}. \tag{3.11}$$

In (3.9), (3.10) and (3.11), $A^m(k)$, $B^m(k)$ and $P^m(k)$ are arbitrary functions of k only.

Substituting (3.10) and (3.11) into the Fourier transform of the Stokes continuity equation (3.3b):

$$\partial_x \hat{u}_1^m + ik\hat{u}_2^m = 0,$$

we can find the relationship

$$B^m(k) = \frac{i}{k} A^m(k) \left(k^2 + \frac{1}{\mu_f \, \theta \, \Delta t} \right)^{1/2}. \tag{3.12}$$

Moreover, the Fourier transform of the Beavers–Joseph–Saffman condition (3.3c) is

$$-\mu_f \left(\partial_x \hat{u}_2^m + ik \, \hat{u}_1^m \right) = \xi_f \, \hat{u}_2^m.$$

Using (3.10) and (3.11) at $\{0\} \times \mathbb{R}$, and the relationship (3.12), we find

$$P^m(k) = A^m(k) \, \mathcal{F}(k) \tag{3.13}$$

with $\mathcal{F}(k)$ defined as in (3.8).

Taking now the Fourier transform of the Darcy equation (3.4a), we find

$$\frac{S_p}{\Delta t} \hat{p}_p^m - \theta \, \eta_1 \partial_{xx} \hat{p}_p^m + \theta \, \eta_2 \, k^2 \hat{p}_p^m = 0,$$

or, equivalently,

$$\partial_{xx} \hat{p}_p^m - \frac{\eta_2}{\eta_1} \left(k^2 + \frac{S_p}{\eta_2 \, \theta \, \Delta t} \right) \hat{p}_p^m = 0,$$

whose general solution is

$$\hat{p}_p^m(x,k) = \Phi^m(k) \, e^{-\left(\frac{\eta_2}{\eta_1} \left(k^2 + \frac{S_p}{\eta_2 \, \theta \, \Delta t} \right) \right)^{1/2} x}. \tag{3.14}$$

The Fourier transforms of the interface conditions (3.3d) and (3.4b) become

$$\left(-2\mu_f \partial_x \hat{u}_1^m + \hat{p}_f^m \right) - \alpha_f \, \hat{u}_1^m = \hat{p}_p^{m-1} - \alpha_f \left(-\eta_1 \, \partial_x \hat{p}_p^{m-1} \right), \tag{3.15}$$

$$\hat{p}_p^m + \alpha_p \left(-\eta_1 \, \partial_x \hat{p}_p^m \right) = \left(-2\mu_f \partial_x \hat{u}_1^m + \hat{p}_f^m \right) + \alpha_p \, \hat{u}_1^m. \tag{3.16}$$

Using the expressions (3.9)–(3.11), (3.14) at $\{0\} \times \mathbb{R}$ and the relationships (3.12) and (3.13), from (3.15) and (3.16) we obtain, respectively,

$$\left(-\left(\alpha_f + 2\mu_f\left(k^2 + \frac{1}{\mu_f\,\theta\,\Delta t}\right)^{\frac{1}{2}}\right) + \left(2\mu_f k^2 \Delta t + \alpha_f |k| \Delta t + 1\right)\,\mathcal{F}(k)\right) A^m(k)$$
$$= \left(1 - \alpha_f\,\eta_p\left(k^2 + \frac{S_p}{\eta_2\,\theta\,\Delta t}\right)^{\frac{1}{2}}\right) \Phi^{m-1}(k), \tag{3.17}$$

$$\left(1 + \alpha_p\,\eta_p\left(k^2 + \frac{S_p}{\eta_2\,\theta\,\Delta t}\right)^{\frac{1}{2}}\right) \Phi^m(k)$$
$$= \left(\left(\alpha_p - 2\mu_f\left(k^2 + \frac{1}{\mu_f\,\theta\,\Delta t}\right)^{\frac{1}{2}}\right) + \left(2\mu_f k^2 \Delta t - \alpha_p |k| \Delta t + 1\right)\,\mathcal{F}(k)\right) A^m(k). \tag{3.18}$$

The convergence factor (3.5) can now be directly obtained from (3.17) and (3.18), using the definitions (3.6) and (3.7).

A direct calculation shows that $1 - |k|\,\Delta t\,\mathcal{F}(k) < 0$ for all $k \neq 0$, so that $\mathcal{H}(k)$ is well defined. □

REMARK 3.2 Proposition 3.1 explicitly excludes the frequency $k = 0$. In fact, in this case, the only admissible Stokes pressure $\hat{p}_f^m(x,k)$ would be the zero function since it must satisfy the homogeneous Laplace equation $-\partial_{xx}\hat{p}_f^m = 0$ in the infinite half plane Ω_f, and decay at infinity in order to be L^2 integrable. The velocities would become $\widehat{u}_1^m(x,k) = A^m(k)\,e^{\sqrt{\frac{1}{\mu_f\theta\Delta t}}x}$, and $\widehat{u}_2^m(x,k) = B^m(k)\,e^{\sqrt{\frac{1}{\mu_f\theta\Delta t}}x}$. Inserting these expressions into the divergence-free constraint and into the Beavers–Joseph–Saffman condition finally leads to $\widehat{u}_1^m(x,k) = \widehat{u}_2^m(x,k) = 0$. The frequency $k = 0$ must be accounted for if one considers periodic boundary conditions in a bounded domain in the y-direction as in Gander & Vanzan (2020a). In such a case, due to boundedness of the domain, one obtains $\widehat{u}_1^m = \widehat{u}_2^m = 0, \widehat{p}_f^m(x,k) = P^m \in \mathbb{R}$, and $\widehat{p}_p^m(x,k) = \Phi^m(k)\,e^{-\sqrt{\frac{S_p}{\theta\eta_1\Delta t}}x}$. Inserting these expressions into the transmission conditions, we obtain $\rho(k=0,\alpha_f,\alpha_p) = \frac{1-\alpha_f\eta_p\sqrt{\frac{S_p}{\theta\eta_2\Delta t}}}{1+\alpha_p\eta_p\sqrt{\frac{S_p}{\theta\eta_2\Delta t}}}$.

Now, our goal is to characterize optimal parameters α_f and α_p that minimize the convergence factor (3.5). To this aim, we study the min-max problem

$$\min_{\alpha_f,\alpha_p\in\mathbb{R}^+} \max_{[k_{\min},k_{\max}]} |\rho(k,\alpha_f,\alpha_p)|, \tag{3.19}$$

where $[k_{\min}, k_{\max}]$ is the range of frequencies of interest for the problem, and they are usually approximated by $k_{\min} = \frac{\pi}{|\Gamma|}$ and $k_{\max} = \frac{\pi}{h}$, where h is the mesh size (Gander, 2006).

3.2 *Optimization of the convergence factor in a simplified setting*

The solution of the min-max problem (3.19) is quite challenging, and it significantly differs from several min-max problems studied in the literature (see Gander, 2006; Gander *et al.*, 2007; Gander & Vanzan, 2019, 2020b, and references therein). Moreover, the expression of $\mathcal{F}(k)$ is quite complex and it prevents the use of direct calculations. Therefore, in order to make the min-max problem (3.19) feasible of a theoretical study, we make two simplifications. First, we replace the Beavers–Joseph–Saffman condition (2.3c) by the zero tangential interface velocity

$$(\mathbf{u}_f)_\tau = 0 \quad \text{on } \Gamma, \tag{3.20}$$

which corresponds to the limit $\xi_f \to \infty$ in (2.3c). This simplification was considered also, e.g., in D'Angelo & Zunino (2011) in the context of modelling blood perfusion, and it is motivated by the fact that the fluid velocity significantly decreases in the neighborhood of the porous medium where, in the first approximation, the flow is as if the porous medium was impervious (see, e.g., Ene & Sanchez-Palencia, 1975; Levy & Sanchez-Palencia, 1975; Layton *et al.*, 2003). Although this approximation is used to estimate optimal parameters α_f and α_p, numerical results in Section 4 show that such coefficients provide a robust method also for the Beavers–Joseph–Saffman condition (2.3c). Considering (3.20), we find

$$\lim_{\xi_f \to \infty} \mathcal{F}(k) = \frac{\left(k^2 + \frac{1}{\mu_f\, \theta\, \Delta t}\right)^{\frac{1}{2}}}{k^2\, \Delta t}.$$

Using this limit in (3.7), we obtain the simplified expression

$$\mathcal{H}(k) = \frac{\left(k^2 + \frac{1}{\mu_f\, \theta\, \Delta t}\right)^{\frac{1}{2}}}{|k|\, \Delta t \left(\left(k^2 + \frac{1}{\mu_f\, \theta\, \Delta t}\right)^{\frac{1}{2}} - |k|\right)}. \tag{3.21}$$

Second, instead of minimizing over two free parameters α_f, α_p, we would like to set $\alpha_f = \mathcal{G}(s)$ and $\alpha_p = \mathcal{H}(s)$, for a $s \in \mathbb{R}^+$ following Gander & Vanzan (2017, 2019). In this way, the minimization problem (3.19) becomes

$$\min_{s \in \mathbb{R}^+} \max_{[k_{\min}, k_{\max}]} |\rho(k, s)|$$

with

$$\rho(k, s) = \frac{\mathcal{G}(k) - \mathcal{G}(s)}{\mathcal{G}(k) + \mathcal{H}(s)} \cdot \frac{\mathcal{H}(k) - \mathcal{H}(s)}{\mathcal{H}(k) + \mathcal{G}(s)}.$$

The motivation for this parametrization is that, if the functions $\mathcal{G}(\cdot)$ and $\mathcal{H}(\cdot)$ are strictly monotonic, the convergence factor has only one zero for $k > 0$ located at $k = s$. Then, analyzing the derivative of $\rho(k, s)$ with respect to s, one can conclude that the optimal parameter, say s_{opt}, is the one leading to an equioscillation between the convergence factor at $k_{\min}$ and $k_{\max}$, i.e., $|\rho(k_{\min}, s_{opt})| = |\rho(k_{\max}, s_{opt})|$,

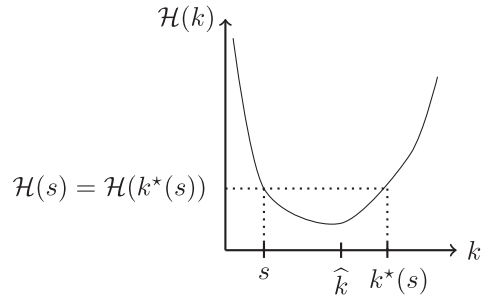

FIG. 2. Sketch of the graph of the function $\mathcal{H}(k)$.

so that $\alpha_f = \mathcal{G}(s_{opt})$ and $\alpha_p = \mathcal{H}(s_{opt})$. The key point of this strategy is that both $\mathcal{G}(\cdot)$ and $\mathcal{H}(\cdot)$ must be strictly monotonic, so that the convergence factor has as many zeros as the parameters to optimize.

For the problem at hand, this approach is not viable. The function $k \mapsto \mathcal{G}(k)$ in (3.6) is strictly positive and decreasing $\forall k > 0$, but the map $k \mapsto \mathcal{H}(k)$ in (3.21) is strictly positive, decreasing for $k < \widehat{k}$ and increasing for $k > \widehat{k}$, where

$$\widehat{k} = \frac{\sqrt{2}}{2}\sqrt{\frac{\sqrt{5}-1}{\mu_f\,\theta\,\Delta t}}, \tag{3.22}$$

with $\lim_{k\to+\infty} \mathcal{H}(k) = +\infty$ and $\lim_{k\to 0^+} \mathcal{H}(k) = +\infty$. Hence, upon setting $\alpha_f = \mathcal{G}(s)$ and $\alpha_p = \mathcal{H}(s)$, the convergence factor would have two zeros for $k > 0$, one at $k = s$ (for which both $\mathcal{G}(k) - \mathcal{G}(s) = 0$ and $\mathcal{H}(k) - \mathcal{H}(s) = 0$) and another one at the unique point, say $k^\star(s)$, such that $\mathcal{H}(k^\star(s)) = \mathcal{H}(s)$; see Fig. 2. Only for $s = \widehat{k}$, one has $k^\star(\widehat{k}) = \widehat{k}$.

Therefore, the additional difficulty of performing symbolic calculations with the expressions of $\mathcal{G}$ and $\mathcal{H}$ suggests us to simplify the problem by setting $\alpha_p = \mathcal{H}(\widehat{k}) =: l$ (i.e., we set α_p equal to the value of $\mathcal{H}(\cdot)$ at the minimum $\widehat{k}$) while leaving $\alpha_f = \mathcal{G}(s)$ with $s \in \mathbb{R}^+$. In this way, the expression of $\rho(k, \alpha_f, \alpha_p)$ in (3.5) becomes

$$\rho(k,s) = \frac{\mathcal{G}(k) - \mathcal{G}(s)}{\mathcal{H}(k) + \mathcal{G}(s)} \cdot \frac{\mathcal{H}(k) - l}{\mathcal{G}(k) + l}, \tag{3.23}$$

with two zeros, one fixed at $k = \widehat{k}$, the other at $k = s$, which remains the only one zero that depends on the parameter s.

Thus, instead of (3.19), we consider the min-max problem

$$\min_{s\in\mathbb{R}^+} \max_{k\in[k_{\min},k_{\max}]} |\rho(k,s)| \tag{3.24}$$

with $\rho(k,s)$ defined in (3.23), and where $l = \mathcal{H}(\widehat{k})$ while $\widehat{k}$ is defined in (3.22).

REMARK 3.3 Setting $\alpha_p = l$ does not necessarily lead to less efficient transmission conditions than choosing $\alpha_p = \mathcal{H}(s)$ and then optimizing also α_p. In fact, despite in the latter case one apparently optimizes both α_p and α_f, these parameters are actually constrained to move on the one dimensional

curve $\Sigma := \left\{(x,y) \in \mathbb{R}^+ : (x,y) = (\mathcal{G}(s), \mathcal{H}(s)),\ s \in \mathbb{R}^+\right\}$ and $\rho(k,s)$ has a single zero at $k = s$. In our setting instead, $\rho(k,s)$ has two zeros, one located at at $\widehat{k}$ which is fixed and depends exclusively on the physical and discretization parameters μ_f, θ and Δt. The second zero is located at $k = s$, and it is optimized taking into account the position of the first one.

The following theorem characterizes the optimal solution of (3.24) according to the position of $\widehat{k}$ with respect to $[k_{\min}, k_{\max}]$.

THEOREM 3.4 The solution of the min-max problem (3.24) can be characterized as indicated in the cases below.

- Case $\widehat{k} \in [k_{\min}, k_{\max}]$.
  - The solution of (3.24) is the unique $s_1^\star$ such that $|\rho(k_{\min}, s_1^\star)| = |\rho(k_{\max}, s_1^\star)| =: M$, if $|\rho(\widetilde{k}(s_1^\star), s_1^\star)| \leq M$, where $\widetilde{k}$ is the unique local maximum of $|\rho(k,s)|$ in $[k_{\min}, k_{\max}]$.
  - If $|\rho(\widetilde{k}(s_1^\star), s_1^\star)| > M$ and $s_1^\star < \widehat{k}$, the optimal solution is the unique value $s_2^\star$ in the interval $s_1^\star < s < \widehat{k}$ such that $|\rho(k_{\min}, s_2^\star)| = |\rho(\widetilde{k}, s_2^\star)|$.
  - If $|\rho(\widetilde{k}(s_1^\star), s_1^\star)| > M$ and $s_1^\star > \widehat{k}$, the optimal solution is the unique value $s_3^\star$ in the interval $\widehat{k} < s < s_1^\star$ such that $|\rho(k_{\max}, s_3^\star)| = |\rho(\widetilde{k}, s_3^\star)|$.
- Case $\widehat{k} > k_{\max}$.
  - The solution of (3.24) is the unique $s_1^\star$ such that $|\rho(k_{\min}, s_1^\star)| = |\rho(k_{\max}, s_1^\star)|$, if $\widetilde{k}(s_1^\star) > k_{\max}$.
  - If $\widetilde{k}(s_1^\star) < k_{\max}$, the optimal solution is the unique value $s_4^\star$ such that $|\rho(k_{\min}, s_4^\star)| = |\rho(\widetilde{k}, s_4^\star)|$.
- Case $\widehat{k} < k_{\min}$.
  - The solution of (3.24) is the unique $s_1^\star$ such that $|\rho(k_{\min}, s_1^\star)| = |\rho(k_{\max}, s_1^\star)|$, if $\widetilde{k}(s_1^\star) < k_{\min}$.
  - If $\widetilde{k}(s_1^\star) > k_{\min}$, the optimal solution is the unique $s_5^\star$ such that $|\rho(\widetilde{k}, s_5^\star)| = |\rho(k_{\max}, s_5^\star)|$.

Proof. Let us start with a preliminary analysis of $\mathcal{H}(\cdot)$ and $\rho(\cdot,\cdot)$. As observed above, $\mathcal{H}(k)$ is a strictly decreasing function for $k < \widehat{k}$, strictly increasing for $k > \widehat{k}$, and with minimum at $k = \widehat{k}$. Thus, $(\mathcal{H}(k) - l)$ is nonnegative for every k, and $\rho(k,s)$ has two zeros, the one first at $k = s$ and the second one fixed at $k = \widehat{k}$. Further, $\rho(k,s)$ is positive for $k < s$ and negative for $k > s$.

The sign of the partial derivative with respect to s is equal to

$$\operatorname{sign}\left(\frac{\partial|\rho(k,s)|}{\partial s}\right) = \operatorname{sign}(\rho(k,s))\ \operatorname{sign}\left(\frac{\mathcal{G}'(s)(l-\mathcal{H}(k))(\mathcal{H}(k)+\mathcal{G}(k))}{(\mathcal{G}(k)+l)(\mathcal{H}(k)+\mathcal{G}(s))^2}\right).$$

Being the second term on the right-hand side always positive since $(l - \mathcal{H}(k)) < 0$ and $\mathcal{G}$ is strictly decreasing, there holds

$$\operatorname{sign}\left(\frac{\partial|\rho(k,s)|}{\partial s}\right) = \operatorname{sign}(\rho(k,s)) = \operatorname{sign}(s-k).$$

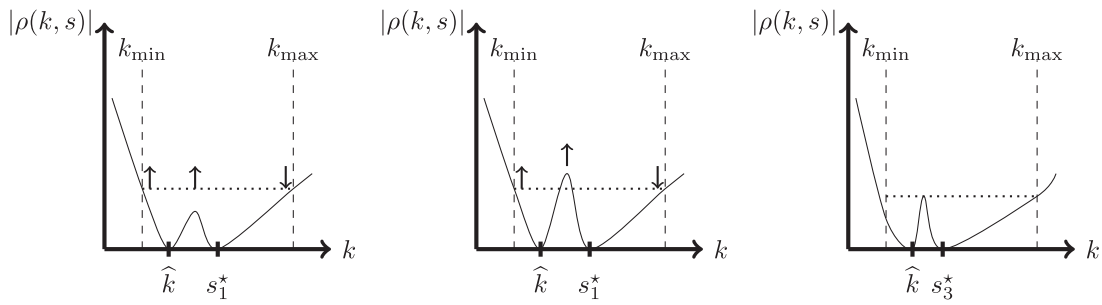

FIG. 3. The three panels support the proof of Theorem 3.4. The black arrows show how $|\rho(k,s)|$ behaves in the three local maxima as s increases. In the left panel, equioscillating between $|\rho(k_{\min},s)|$ and $|\rho(k_{\max},s)|$ leads to an optimal solution. In the central panel, $s_1^\star$ is not optimal, as decreasing s would decrease $|\rho|$ at both $k_{\min}$ and $\widetilde{k}$ and increase it at $k_{\max}$ until $|\rho(\widetilde{k},s)| = |\rho(k_{\max},s)|$.

We conclude that the optimal s must be greater than $k_{\min}$, since otherwise we would have $\operatorname{sign}\left(\frac{\partial|\rho(k,s)|}{\partial s}\right) < 0$ for every $k \in \left[k_{\min}, k_{\max}\right]$, hence we could not be at the optimum, since increasing s would decrease $|\rho(k,s)|$ for all $k \in [k_{\min}, k_{\max}]$. For analogous reasons, the optimal s must be less than $k_{\max}$, so that we can restrict the range of s to the interval $\left[k_{\min}, k_{\max}\right]$. Studying the derivative with respect to k, one notices that $|\rho(k,s)|$ is decreasing for $k \leq \min\{s, \widehat{k}\}$ and increasing for $k \geq \max\{s, \widehat{k}\}$. Between the two zeros, it has a unique local maximum in $\widetilde{k}(s)$.

Let us now suppose that $\widehat{k} \in \left[k_{\min}, k_{\max}\right]$. Since $s \in \left[k_{\min}, k_{\max}\right]$, the local maximum $\widetilde{k}(s)$ surely lies in $\left[k_{\min}, k_{\max}\right]$. The min-max problem (3.24) then simplifies to

$$\min_{s\in\mathbb{R}^+} \max_{k\in[k_{\min},k_{\max}]} |\rho(k,s)| = \min_{s\in[k_{\min},k_{\max}]} \max\left\{\left|\rho(k_{\min},s)\right|, \rho(\widetilde{k}(s),s)\right|, \left|\rho\left(k_{\max},s\right)\right|\right\}.$$

We now study how $\left|\rho\left(k_{\min},s\right)\right|$ and $\left|\rho\left(k_{\max},s\right)\right|$ depend on s. For all $s \in \left(k_{\min}, k_{\max}\right]$, there holds

$$\operatorname{sign}\left(\frac{\partial|\rho(k,s)|}{\partial s}|_{k=k_{\min}}\right) = \operatorname{sign}\left(s-k_{\min}\right) > 0, \quad \operatorname{sign}\left(\frac{\partial|\rho(k,s)|}{\partial s}|_{k=k_{\max}}\right) = \operatorname{sign}\left(s-k_{\max}\right) < 0.$$

Thus, $|\rho(k_{\min},s)|$ is a strictly increasing function of s that satisfies $\left|\rho\left(k_{\min},k_{\min}\right)\right| = 0$ and $\left|\rho\left(k_{\min},k_{\max}\right)\right| > 0$. Similarly, $|\rho(k_{\max},s)|$ is strictly decreasing, with $|\rho(k_{\max},k_{\min})| > 0$ and $|\rho(k_{\max},k_{\max})| = 0$. By continuity there exists a unique $s_1^\star$ such that $|\rho(k_{\min},s_1^\star)| = |\rho(k_{\max},s_1^\star)| =: M$. Now, if $|\rho(\widetilde{k}(s_1^\star),s_1^\star)| \leq M$, we have found the optimum, since perturbing s would increase either $|\rho(k_{\min},s)|$, or $|\rho(k_{\max},s)|$, and thus the maximum of $|\rho(k,s)|$, see left panel of Fig. 3. Suppose instead that $|\rho(\widetilde{k}(s_1^\star),s_1^\star)| > M$. In this case, the optimal solution is obtained by equioscillating $|\rho(\widetilde{k}(s),s)|$ either with $|\rho(k_{\min},s)|$ or $|\rho(k_{\max},s)|$, since they are respectively strictly increasing and strictly decreasing with respect to s (central panel of Fig. 3). Further, the total derivative of $|\rho(\widetilde{k}(s),s)|$ with respect to s is

$$\frac{d|\rho(\widetilde{k}(s),s)|}{ds} = \operatorname{sign}(s-k)\left(\frac{\partial|\rho(k,s)|}{\partial k}|_{k=\widetilde{k}(s)} \cdot \widetilde{k}'(s) + \frac{\partial\rho(\widetilde{k}(s),s)}{\partial s}\right) = \operatorname{sign}(s-k)\frac{\partial\rho(\widetilde{k}(s),s)}{\partial s},$$

whose sign is

$$\operatorname{sign}\left(\frac{d|\rho(\widetilde{k}(s),s)|}{ds}\right) = \operatorname{sign}(s-k).$$

If $s_1^\star < \widehat{k}$ and $|\rho(\widetilde{k}(s_1^\star), s_1^\star)| > M$, decreasing s in the range $[k_{\min}, s_1^\star]$ would not improve the maximum of the convergence factor as $|\rho(\widetilde{k}(s), s)|$ increases. On the other hand, increasing s in the range $[s_1^\star, \widehat{k}]$ would increase $|\rho(k_{\min}, s)|$ and decrease both $|\rho(\widetilde{k}, s)|$ and $|\rho(k_{\max}, s)|$. There exists surely $s_2^\star \in [s_1^\star, \widehat{k}]$ for which $|\rho(\widetilde{k}(s_2^\star), s_2^\star)| = |\rho(k_{\min}, s_2^\star)|$ since $|\rho(\widetilde{k}(\widehat{k}), \widehat{k})| = 0$. The optimal solution is then $s_2^\star$ as increasing further s would increase $|\rho(k_{\min}, s)|$ as well. Similarly, one shows that if $s_1^\star > \widehat{k}$, the optimal solution is given by $s_3^\star \in [\widehat{k}, s_1^\star]$ such that $|\rho(\widetilde{k}(s), s)| = |\rho(k_{\max}, s)|$ (right panel of Fig. 3). This ends the proof of the first claim.

Next, suppose that $\widehat{k} > k_{\max}$, so that the local maximum $\widetilde{k}(s)$ is not necessarily in $[k_{\min}, k_{\max}]$. Let us define $s_4^\star \in [k_{\min}, k_{\max}]$ be the unique solution of $|\rho(k_{\min}, s)| = |\rho(k_{\max}, s)|$. If $\widetilde{k}(s_4^\star) > k_{\max}$, then $s_4^\star$ is the optimal solution as varying s would increase either $|\rho(k_{\min}, s)|$ or $|\rho(k_{\max}, s)|$. In contrast, if $\widetilde{k}(s_4^\star) < k_{\max}$, then $|\rho(\widetilde{k}(s_4^\star), s_4^\star)| > |\rho(k_{\min}, s_4^\star)|$ and it is convenient to increase s until $|\rho(\widetilde{k}(s), s)| = |\rho(k_{\min}, s)|$. The case $\widehat{k} < k_{\min}$ is treated similarly. □

REMARK 3.5 Theorem 3.4 considers three cases depending on the relative position of $\widehat{k}$ with respect to $[k_{\min}, k_{\max}]$. This can be easily determined and it depends on few physical, geometrical and discretization parameters. Using the standard ansatzes $k_{\min} = \frac{\pi}{|\Gamma|}$ and $k_{\max} = \frac{\pi}{h}$ (Gander, 2006), from (3.22) we get

$$\begin{aligned}
&\widehat{k} < k_{\min} && \text{if} \quad \mu_f \theta \Delta t > \tfrac{(\sqrt{5}-1)|\Gamma|^2}{2\pi^2},\\
&k_{\min} \le \widehat{k} \le k_{\max} && \text{if} \quad \tfrac{(\sqrt{5}-1)h^2}{2\pi^2} \le \mu_f \theta \Delta t \le \tfrac{(\sqrt{5}-1)|\Gamma|^2}{2\pi^2},\\
&\widehat{k} > k_{\max} && \text{if} \quad \mu_f \theta \Delta t < \tfrac{(\sqrt{5}-1)h^2}{2\pi^2}.
\end{aligned}$$

Notice that $\widehat{k} < k_{\min}$ poses a tight constraint on the value of Δt, which is not likely to be satisfied in practice. The other two cases are more realistic, and the specific regime depends on the choice of Δt and h which is dictated by the finite element spaces and the time integration scheme used.

To conclude this section, we study how the optimized contraction factor behaves as $h \to 0$. Unfortunately, asymptotic expansions do not lead to simplified formulae neither for the optimized parameter nor for the optimized convergence factor. Thus, we report a numerical study in Table 1. We consider physical relevant values for the parameters (see Section 4.1) and two fixed values for the time discretization. We remark that Theorem 3.4 leads to an optimized Schwarz method which exhibits a mesh-independent convergence, since the convergence factor converges to a finite quantity strictly smaller than 1, as $h \to 0$. This remarkable property of optimized Schwarz method has already been proven for the coupling of heterogeneous second-order PDEs, Gander & Vanzan (2019), but does not hold in general when coupling equations described by the same differential operator. The numerical experiments reported in the next section confirm this property on a wide range of test cases.

4. Numerical results

In this section, we discuss numerical results to test the proposed framework. Subsection 4.1 introduces the physical relevant parameters used in the simulations. Subsection 4.2 validates the Fourier analysis

TABLE 1 *Behaviour of the optimized parameter and convergence factor as* $h \to 0$. *Parameters:* $\eta_p = 4 \times 10^{-6}$, $S_p = 4 \times 10^{-15}$, $Re = 1$, $\theta = 0.5$, $k_{\min} = \pi$, $k_{\max} = \frac{\pi}{h}$. *Top table:* $\Delta t = 0.01$. *Bottom table:* $\Delta t = 10^{-4}$

h	$s^\star$	α_f	α_p	$\max_{k\in[k_{\min},k_{\max}]} \lvert\rho(k,s^\star)\rvert$
10^{-2}	2.5×10^2	9.8×10^2	4.7×10^1	0.08
10^{-3}	1.6×10^3	1.5×10^2	4.7×10^1	0.56
10^{-4}	5.0×10^3	4.9×10^1	4.7×10^1	0.75
10^{-6}	6.7×10^3	3.7×10^1	4.7×10^1	0.78
10^{-8}	6.7×10^3	3.7×10^1	4.7×10^1	0.78
h	$s^\star$	α_f	α_p	$\max_{k\in[k_{\min},k_{\max}]} \lvert\rho(k,s^\star)\rvert$
10^{-2}	1.3×10^1	1.8×10^4	4.7×10^2	0.18
10^{-3}	3.9×10^2	6.2×10^2	4.7×10^2	0.83
10^{-4}	5.8×10^3	4.2×10^2	4.7×10^2	0.86
10^{-6}	6.1×10^3	4.2×10^2	4.7×10^2	0.86
10^{-8}	6.1×10^3	4.2×10^2	4.7×10^2	0.86

by considering the Stokes–Darcy coupling on a bounded domain with periodic boundary conditions and with zero tangential velocity, so to mimic the hypothesis of Section 3. Next, in subsection 4.3 we violate the assumptions of the Fourier analysis by considering nonperiodic boundary conditions, together with the Beavers–Joseph–Saffman boundary condition. Finally in subsection 4.4, we present the convergence of the Robin–Robin method for a realistic application.

4.1 *Choice of physically relevant parameters*

For the numerical tests we consider an incompressible fluid with kinematic viscosity $\nu = 10^{-6}$ m^2/s (water) at Reynolds $0.1 \leq Re \leq 5$, and we choose the characteristic dimension of the domain Ω_f to be $X_f = 0.05$ m. For Darcy's problem, the dimensionless coefficient S_p is obtained as $S_p = \nu^2 \frac{S_0}{g} \frac{Re^2}{X_f^2}$, where $g = 9.8\ \text{m} \times \text{s}^{-2}$ is the magnitude of the gravity acceleration, and S_0 is the specific storage whose value ranges, e.g., in the interval $10^{-5}\ \text{m}^{-1} \leq S_0 \leq 10^{-3}\ \text{m}^{-1}$ (Moraiti, 2012). The porous medium is characterized by constant intrinsic permeability $\mathbf{K}$ in the range $10^{-11}\ \text{m}^2 \leq \mathbf{K} \leq 10^{-8}\ \text{m}^2$ (Bear, 1979), so that $\boldsymbol{\eta}_p = \frac{\mathbf{K}}{X_f^2} Re$ is also constant with $\eta_1 = \eta_2$. Using the indicated values, we identify four test cases (A)–(D) with parameters of physical relevance that we will use for our numerical experiments. The test cases are reported in Table 2 with values of the dimensionless quantities rounded to 2 decimal places.

4.2 *Tests with periodic boundary conditions*

Consider the domain $\Omega = (0,1) \times (-1,1)$ decomposed into $\Omega_f = (0,1)^2$ and $\Omega_p = (0,1) \times (-1,0)$, with $\Gamma = (0,1) \times \{0\}$. The discretization is based on a uniform mesh of squares of edge length $h_j = 0.1 \times 2^{1-j}$ $j = 1, \ldots, 4$. Each square is then divided into two right triangles. We use Taylor–Hood finite elements for Stokes and continuous Lagrangian $\mathbb{P}_2$ finite elements for Darcy's pressure. For the time discretization we use the Crank–Nicolson method ($\theta = \frac{1}{2}$). We impose homogeneous Dirichlet boundary conditions on the

TABLE 2 *Values of the dimensionless parameters defining four test cases (A)–(D)*

Test	(A)	(B)	(C)	(D)
Re	0.1	1	0.1	5
S_p	4.08×10^{-16}	4.08×10^{-15}	4.08×10^{-18}	1.02×10^{-14}
η_p	4.00×10^{-10}	4.00×10^{-7}	4.00×10^{-9}	2.00×10^{-7}
ξ_f	$1.58 \times 10^{+5}$	$1.58 \times 10^{+3}$	$5.00 \times 10^{+4}$	$1.00 \times 10^{+3}$

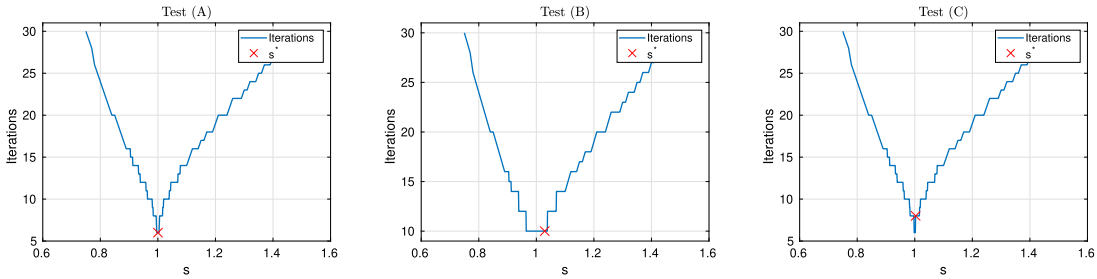

FIG. 4. Number of iterations to reach a relative tolerance of 10^{-8}.

horizontal edges of Ω and periodic boundary conditions on the vertical edges, which permit to mimic the assumption on the unboundedness of the domain required by the Fourier analysis; see Gander & Vanzan (2020a). In this setting, we consider the error equation (i.e., $\chi_f^n = 0$, $\chi_p^n = 0$ in (2.14)) and study the convergence of the parallel version of the stationary iteration (2.13) to the zero solution starting from a random initial guess. Theorem 3.4 does not cover the case under study as we need to include the zero frequency $k = 0$. We thus compute the optimized value of s by solving numerically the min-max problem $\min_{s\in\mathbb{R}} \max_{k\in\{0\}\cup[k_{\min},k_{\max}]} |\rho(k,s)|$ using the Nelder–Mead algorithm (Lacis & Bagheri, 2017). To do so, for a given s we evaluate $|\rho(k,s)|$ on a discretized grid $\mathcal{K}$ of the set $\{0\} \cup [k_{\min}, k_{\max}]$ and then call the optimization routine to minimize the function $s \to \max_{k\in\mathcal{K}} |\rho(k,s)|$. Table 3 reports the values of the optimal parameters α_f, α_p, and the number of iterations to reach a tolerance of 10^{-8} on the relative error of the stationary iterations for different values of h_j and for timesteps $\Delta t_1 = 0.05$, $\Delta t_2 = 0.01$, $\Delta t_3 = 0.005$ and $\Delta t_4 = 0.001$. Notice that very large values of α_f essentially transform the Robin–Robin algorithm into a Dirichlet–Robin algorithm, in which the Stokes subdomain receives the Darcy velocity as boundary conditions at the interface Γ.

Figure 4 reports the number of iterations to solve the coupled system (2.13) up to a relative tolerance of 10^{-8} for tests (A), (B) and (C). The discretization parameters are $h = 1/32$, $\Delta t = 0.01$ and $\theta = 0.5$. Notice that the optimized parameter $s^\star$ obtained by minimizing $\min_{s\in\mathbb{R}} \max_{k\in\{0\}\cup[k_{\min},k_{\max}]} |\rho(k,s)|$ always leads to an optimal numerical convergence, thus validating numerically Proposition 3.1.

4.3 *Tests with analytic solution*

Consider the domain $\Omega_f = (0, 0.5) \times (1, 1.5)$, $\Omega_p = (0, 0.5) \times (0.5, 1)$ with interface $\Gamma = (0, 0.5) \times \{1\}$, and the time interval $[0, 0.5]$. The boundary conditions and forces $\mathbf{f}_f$ and f_p are chosen in such a way that the exact solution of the problem is $\mathbf{u}_f = (\sqrt{\mu_f \eta_p} \cos(t), \alpha_{BJ} x \cos(t))$, $p_f = (2\mu_f(x + y - 1) +$

TABLE 3 *Optimal parameters α_f, α_p and number of stationary iterations to reach a tolerance of* 10^{-8}. *On the top Table* $\Delta t = 0.01$, *on the bottom Table* $h = 1/16$

Test	Mesh	α_f	α_p	iter
(A)	h_1	$2.50 \times 10^{+9}$	$1.49 \times 10^{+2}$	4
	h_2	$2.50 \times 10^{+9}$	$1.49 \times 10^{+2}$	4
	h_3	$2.50 \times 10^{+9}$	$1.49 \times 10^{+2}$	6
	h_4	$2.49 \times 10^{+9}$	$1.49 \times 10^{+2}$	6
(B)	h_1	$2.49 \times 10^{+6}$	$4.71 \times 10^{+1}$	6
	h_2	$2.47 \times 10^{+6}$	$4.70 \times 10^{+1}$	8
	h_3	$2.39 \times 10^{+6}$	$4.71 \times 10^{+1}$	12
	h_4	$2.02 \times 10^{+6}$	$4.71 \times 10^{+1}$	20
(C)	h_1	$2.50 \times 10^{+8}$	$1.49 \times 10^{+2}$	6
	h_2	$2.50 \times 10^{+8}$	$1.49 \times 10^{+2}$	6
	h_3	$2.49 \times 10^{+8}$	$1.49 \times 10^{+2}$	6
	h_4	$2.45 \times 10^{+8}$	$1.49 \times 10^{+2}$	10
(D)	h_1	$5.00 \times 10^{+6}$	$2.11 \times 10^{+1}$	6
	h_2	$5.00 \times 10^{+6}$	$2.11 \times 10^{+1}$	6
	h_3	$4.98 \times 10^{+6}$	$2.11 \times 10^{+1}$	6
	h_4	$4.91 \times 10^{+6}$	$2.11 \times 10^{+1}$	10
Test	Mesh	α_f	α_p	iter
(A)	Δt_1	$2.50 \times 10^{+9}$	$6.66 \times 10^{+1}$	4
	Δt_2	$2.50 \times 10^{+9}$	$1.49 \times 10^{+2}$	4
	Δt_3	$2.50 \times 10^{+9}$	$2.11 \times 10^{+2}$	4
	Δt_4	$2.50 \times 10^{+9}$	$4.71 \times 10^{+2}$	4
(B)	Δt_1	$2.48 \times 10^{+6}$	$2.11 \times 10^{+1}$	8
	Δt_2	$2.49 \times 10^{+6}$	$4.71 \times 10^{+1}$	8
	Δt_3	$2.49 \times 10^{+6}$	$6.66 \times 10^{+1}$	8
	Δt_4	$2.49 \times 10^{+9}$	$1.49 \times 10^{+2}$	8
(C)	Δt_1	$2.50 \times 10^{+8}$	$6.66 \times 10^{+1}$	6
	Δt_2	$2.50 \times 10^{+8}$	$1.49 \times 10^{+2}$	6
	Δt_3	$2.50 \times 10^{+8}$	$2.11 \times 10^{+2}$	6
	Δt_4	$2.50 \times 10^{+8}$	$4.71 \times 10^{+2}$	6
(D)	Δt_1	$5.00 \times 10^{+6}$	$9.42 \times 10^{+0}$	6
	Δt_2	$5.00 \times 10^{+6}$	$2.11 \times 10^{+1}$	6
	Δt_3	$5.00 \times 10^{+6}$	$2.98 \times 10^{+1}$	6
	Δt_4	$5.00 \times 10^{+6}$	$6.66 \times 10^{+1}$	6

$(3\eta_p)^{-1})\cos(t)$, $p_p = ((-\alpha_{BJ}x(y-1) + y^3/3 - y^2 + y)/\eta_p + 2\mu_f x)\cos(t)$. In this test case, the exact solution satisfies the BJS condition (2.3c) at Γ instead of the simplified condition (3.20).

For the space discretisation we consider $\mathbb{Q}_2 - \mathbb{Q}_1$ elements for Stokes and $\mathbb{Q}_2$ elements for Darcy on uniform, structured computational grids made by rectangles, while for the time discretisation we use the backward Euler method ($\theta = 1$).

TABLE 4 *Optimal parameters α_f, α_p and number of GMRES iterations for four computational meshes and fixed $\Delta t = 0.01$*

Test	Mesh	α_f	α_p	iter t^1	iter t^n
(A)	h_1	$4.73 \times 10^{+7}$	$1.05 \times 10^{+2}$	4	2
	h_2	$2.38 \times 10^{+7}$	$1.05 \times 10^{+2}$	4	2
	h_3	$1.20 \times 10^{+7}$	$1.05 \times 10^{+2}$	4	3
	h_4	$5.99 \times 10^{+6}$	$1.05 \times 10^{+2}$	4	4
(B)	h_1	$4.60 \times 10^{+4}$	$3.33 \times 10^{+1}$	5	4
	h_2	$2.35 \times 10^{+4}$	$3.33 \times 10^{+1}$	6	4
	h_3	$1.20 \times 10^{+4}$	$3.33 \times 10^{+1}$	6	4
	h_4	$6.04 \times 10^{+3}$	$3.33 \times 10^{+1}$	8	5
(C)	h_1	$4.73 \times 10^{+6}$	$1.05 \times 10^{+2}$	4	3
	h_2	$2.38 \times 10^{+6}$	$1.05 \times 10^{+2}$	4	4
	h_3	$1.20 \times 10^{+6}$	$1.05 \times 10^{+2}$	4	4
	h_4	$6.00 \times 10^{+5}$	$1.05 \times 10^{+2}$	6	4
(D)	h_1	$1.17 \times 10^{+5}$	$1.49 \times 10^{+1}$	4	4
	h_2	$4.69 \times 10^{+4}$	$1.49 \times 10^{+1}$	4	4
	h_3	$2.34 \times 10^{+4}$	$1.49 \times 10^{+1}$	6	4
	h_4	$1.19 \times 10^{+4}$	$1.49 \times 10^{+1}$	6	4

First, we test the robustness of the method with respect to the mesh size. For this purpose, we consider four computational meshes with sizes $h_j = 0.1 \times 2^{1-j}, j = 1, \ldots, 4$, and $\Delta t = 0.01$. Then, we test the behaviour of the method with respect to Δt. To this aim, we consider a computational grid with $h = 0.02$ and four timesteps $\Delta t_1 = 0.05$, $\Delta t_2 = 0.01$, $\Delta t_3 = 0.005$ and $\Delta t_4 = 0.001$ as in Section 4.2. In all cases, we solve the interface system (2.14) using GMRES (Saad & Schultz, 1986) with tolerance 10^{-8} on the relative residual starting the iterations from $\lambda_f^0 = 0$ and $\lambda_p^0 = 0$ at the first time step, while at t^n ($n \geq 1$) we set $\lambda_f^{n,0} = \lambda_f^{n-1}$ and $\lambda_p^{n,0} = \lambda_p^{n-1}$. The optimal value of s in (3.24) is computed through a numerical routine that implements the different cases of Theorem 3.4.

Tables 4 and 5 report the values of the optimal parameters α_f and α_p computed for the test cases (A)–(D) and the various discretization parameters, together with the number of iterations needed to solve (2.14) at t^1 and the rounded average number of iterations performed at successive time steps t^n ($n > 1$). The results show that the method is robust with respect to both the discretization parameters h and Δt and to the physical parameters that characterize the time-dependent Stokes–Darcy problem. As already observed in Section 4.2, also in this case we notice that α_f is always few orders of magnitude larger than α_p so that the iterative method behaves like a Dirichlet–Robin one.

4.4 *Tests without analytic solution*

Consider the dimensionless domain $\Omega = (0, 1) \times (0, 1)$ with interface at $y = 0.4$ and Ω_f the upper subdomain, and the dimensionless time interval $[0, t_f]$ with $t_f = 1$. For Darcy's problem, we impose homogeneous Dirichlet boundary condition at the bottom boundary $(0, 1) \times \{0\}$ of the domain, and homogeneous Neumann boundary conditions on the remaining external boundaries of Ω_p. In Ω_f, we impose homogeneous Dirichlet boundary conditions on the external lateral boundaries, while we set

TABLE 5 *Optimal parameters α_f, α_p and number of GMRES iterations for four values of Δt and fixed $h = 0.02$*

Test	Δt	α_f	α_p	iter t^1	iter t^n
(A)	Δt_1	$9.59 \times 10^{+6}$	$4.71 \times 10^{+1}$	4	4
	Δt_2	$9.57 \times 10^{+6}$	$1.05 \times 10^{+2}$	4	3
	Δt_3	$9.56 \times 10^{+6}$	$1.49 \times 10^{+2}$	4	3
	Δt_4	$9.51 \times 10^{+6}$	$3.33 \times 10^{+2}$	4	2
(B)	Δt_1	$9.61 \times 10^{+3}$	$1.49 \times 10^{+1}$	6	5
	Δt_2	$9.56 \times 10^{+3}$	$3.33 \times 10^{+1}$	6	4
	Δt_3	$9.52 \times 10^{+3}$	$4.71 \times 10^{+1}$	7	4
	Δt_4	$9.40 \times 10^{+3}$	$1.05 \times 10^{+2}$	8	4
(C)	Δt_1	$9.60 \times 10^{+5}$	$4.71 \times 10^{+1}$	5	4
	Δt_2	$9.58 \times 10^{+5}$	$1.05 \times 10^{+2}$	5	4
	Δt_3	$9.57 \times 10^{+5}$	$1.49 \times 10^{+2}$	5	4
	Δt_4	$9.51 \times 10^{+5}$	$3.33 \times 10^{+2}$	6	3
(D)	Δt_1	$1.90 \times 10^{+4}$	$6.66 \times 10^{+0}$	6	4
	Δt_2	$1.88 \times 10^{+4}$	$1.49 \times 10^{+1}$	6	4
	Δt_3	$1.87 \times 10^{+4}$	$2.11 \times 10^{+1}$	6	4
	Δt_4	$3.91 \times 10^{+4}$	$4.71 \times 10^{+1}$	6	4

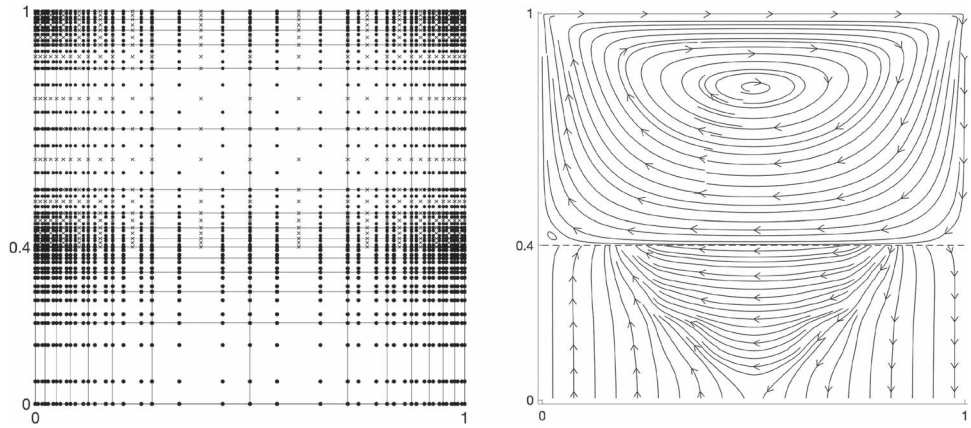

FIG. 5. Sample computational mesh corresponding to $h = h_1$ (left) and representation of the streamlines of the computed solution at $t = 0.75$ using mesh with $h = h_2$.

$\mathbf{u}_f = (u_1, 0)$ on the top boundary $(0, 1) \times \{1\}$ with $u_1 = \min(2U_f\, t/t_f, U_f)$ and dimensionless velocity $U_f = 1$. The forces $\mathbf{f}_f$ and f_p are both zero. The physical parameters are chosen as in tests (A) and (D) of Section 4.1, see Table 2, and the optimized parameters of the iterative methods are computed through a numerical routine that implements the cases of Theorem 3.4.

For the discretization, we use $\mathbb{Q}_3 - \mathbb{Q}_2$ elements for Stokes and $\mathbb{Q}_3$ elements for Darcy with Gauss–Lobatto nodes for the $\mathbb{Q}_3$ polynomials, and the Crank–Nicolson method $\left(\theta = \frac{1}{2}\right)$. The meshes are non-

TABLE 6 *Test of Section 4.4: optimal parameters α_f, α_p and number of GMRES iterations for three non-uniform computational meshes and $\Delta t = 0.05$*

Test	Mesh	No. unknowns at Γ	α_f	α_p	iter t^1	iter t^n
(A)	h_1	86	$2.28 \times 10^{+7}$	$3.33 \times 10^{+1}$	12	9
	h_2	170	$1.14 \times 10^{+7}$	$3.33 \times 10^{+1}$	12	9
	h_3	338	$5.71 \times 10^{+6}$	$3.33 \times 10^{+1}$	14	10
(D)	h_1	86	$4.43 \times 10^{+4}$	4.71	8	7
	h_2	170	$2.25 \times 10^{+4}$	4.71	10	8
	h_3	338	$1.13 \times 10^{+4}$	4.71	12	9

TABLE 7 *Test of Section 4.4: optimal parameters α_f, α_p and number of GMRES iterations for three values of Δt and mesh with h_2*

Test	Δt	α_f	α_p	iter t^1	iter t^n
(A)	Δt_1	$1.14 \times 10^{+7}$	$2.11 \times 10^{+1}$	12	9
	Δt_2	$1.14 \times 10^{+7}$	$2.98 \times 10^{+1}$	12	9
	Δt_3	$1.14 \times 10^{+7}$	$4.21 \times 10^{+1}$	12	9
(D)	Δt_1	$2.26 \times 10^{+4}$	2.98	10	8
	Δt_2	$2.25 \times 10^{+4}$	4.21	10	8
	Δt_3	$2.24 \times 10^{+4}$	5.96	10	8

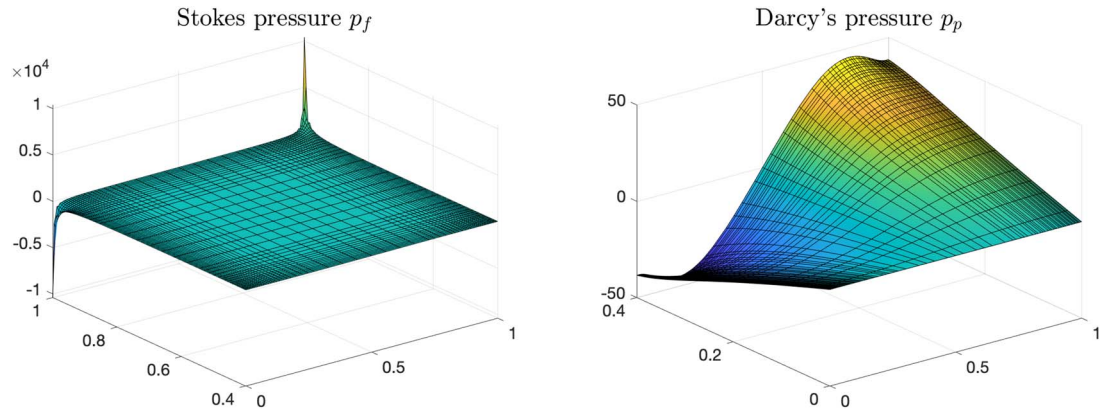

FIG. 6. Stokes pressure p_f (left) and Darcy's pressure p_p (right) computed at $t = 0.75$ using mesh with $h = h_2$.

uniform with smaller elements in the neighbourhood of the external boundary and of the interface. An example is shown in Fig. 5 (left).

Tables 6 and 7 indicate the values of the optimal parameters α_f and α_p and the number of iterations needed to solve (2.14) at t^1 and the rounded average number of iterations performed at successive time steps t^n ($n > 1$). For the computation of the optimal parameters, an average value of h at the interface is

used due to the nonuniformity of the mesh. In Table 6, we set $\Delta t = 0.05$ and we consider three values of h: $h_1 \approx 0.0714$, $h_2 \approx 0.0357$, $h_3 \approx 0.0179$. In Table 7, we consider the mesh characterized by h_2 and we consider three values of Δt: $\Delta t_1 = 0.125$, $\Delta t_2 = 0.0625$, $\Delta t_3 = 0.03125$. As already observed in Section 4.3, the method is robust with respect to both the discretization and the physical parameters and the choice of the optimal parameters α_f and α_p indicate a behaviour analogous to a Dirichlet–Robin algorithm.

Figure 5 (right) and Fig. 6 show the velocity and pressure computed at $t = 0.75$ using the mesh characterized by size h_2 and $\Delta t = 0.05$. (The velocity in Darcy's domain has been postprocessed from the pressure p_p using the MATLAB command 'gradient'.)

5. Conclusions

In this paper, we formulated and analyzed an optimized Schwarz method for the time-dependent Stokes–Darcy problem. Since the convergence factor is different from other cases studied in the literature, we proposed a novel approach to characterize the optimized parameters in the interface Robin conditions in order to guarantee robustness of the iterative method with respect to physical and discretization parameters. Numerical experiments carried out for various configurations of the problem showed the effectiveness of the studied method.

Acknowledgements

The first author acknowledges funding by the EPSRC grant EP/V027603/1.

References

Bear, J. (1979) *Hydraulics of Groundwater*. New York: McGraw-Hill.

Beavers, G. S. & Joseph, D. D. (1967) Boundary conditions at a naturally permeable wall. *J. Fluid Mech.*, **30**, 197–207.

Caiazzo, A., John, V. & Wilbrandt, U. (2014) On classical iterative subdomain methods for the Stokes–Darcy problem. *Comput. Geosci.*, **18**, 711–728.

Cao, Y., Gunzburger, M., He, X. & Wang, X. (2011) Robin–Robin domain decomposition methods for the steady-state Stokes–Darcy system with the Beavers–Joseph interface condition. *Numer. Math.*, **117**, 601–629.

Cao, Y., Gunzburger, M., He, X. & Wang, X. (2014) Parallel, non-iterative, multi-physics domain decomposition methods for time-dependent Stokes–Darcy systems. *Math. Comp.*, **83**, 1617–1644.

Cao, Y., Gunzburger, M., Hu, X., Hua, F., Wang, X. & Zhao, W. (2010) Finite element approximations for Stokes–Darcy flow with Beavers–Joseph interface conditions. *SIAM J. Numer. Anal.*, **47**, 4239–4256.

Çeşmelioğlu, A., Girault, V. & Rivière, B. (2013) Time-dependent coupling of Navier–Stokes and Darcy flows. *ESAIM–Math. Model. Numer. Anal.*, **47**, 539–554.

Chen, W., Gunzburger, M., Hua, F. & Wang, X. (2011) A parallel Robin–Robin domain decomposition method for the Stokes–Darcy system. *SIAM J. Numer. Anal.*, **49**, 1064–1084.

Chen, X., Gander, M. J. & Xu, Y. (2021) Optimized Schwarz methods with elliptical domain decompositions. *J. Sci. Comput.*, **86**, 1–28.

D'Angelo, C. & Zunino, P. (2011) Robust numerical approximation of coupled Stokes' and Darcy's flows applied to vascular hemodynamics and biochemical transport. *ESAIM–Math. Model. Numer. Anal.*, **45**, 447–476.

Discacciati, M. (2004a) *Domain Decomposition Methods for the Coupling of Surface and Groundwater Flows*. PhD thesis. Switzerland: École Polytechnique Fédérale de Lausanne.

Discacciati, M. (2004b) Iterative methods for Stokes/Darcy coupling. *Domain Decomposition Methods in Science and Engineering. Lecture Notes in Computational Science and Engineering (40)* (R. Kornhuber, R. Hoppe, J. Périaux, O. Pironneau, O. Widlund, & J. Xu eds). Berlin and Heidelberg: Springer, pp. 563–570.

Discacciati, M. & Gerardo-Giorda, L. (2018) Optimized Schwarz methods for the Stokes–Darcy coupling. *IMA J. Numer. Anal.*, **38**, 1959–1983.

Discacciati, M., Miglio, E. & Quarteroni, A. (2002) Mathematical and numerical models for coupling surface and groundwater flows. *Appl. Numer. Math.*, **43**, 57–74.

Discacciati, M. & Quarteroni, A. (2004) Convergence analysis of a subdomain iterative method for the finite element approximation of the coupling of stokes and Darcy equations. *Comput. Visual. Sci.*, **6**, 93–103.

Discacciati, M. & Quarteroni, A. (2009) Navier–Stokes/Darcy coupling: modeling, analysis, and numerical approximation. *Rev. Mat. Complut.*, **22**, 315–426.

Discacciati, M., Quarteroni, A. & Valli, A. (2007) Robin–Robin domain decomposition methods for the Stokes–Darcy coupling. *SIAM J. Numer. Anal.*, **45**, 1246–1268.

Dolean, V., Gander, M. J. & Gerardo-Giorda, L. (2009) Optimized Schwarz methods for Maxwell's equations. *SIAM J. Sci. Comput.*, **31**, 2193–2213.

Ene, H. I. & Sanchez-Palencia, E. (1975) Équations et phénomenès de surface pour l'écoulement dans un modèle de milieu poreux. *J. Mécanique*, **14**, 73–108.

Feng, W., He, X., Wang, Z. & Zhang, X. (2012) Non-iterative domain decomposition methods for a non-stationary Stokes–Darcy model with Beavers–Joseph interface conditions. *Appl. Math. Comput.*, **219**, 453–463.

Galvis, J. C. & Sarkis, M. (2007) Balancing domain decomposition methods for mortar coupling Stokes–Darcy systems. *Domain Decomposition Methods in Science and Engineering XVI* (O. B. Widlund & D. E. Keyes eds). Berlin and Heidelberg: Springer, pp. 373–380.

Galvis, J. C. & Sarkis, M. (2010) FETI and BDD preconditioners for Stokes-Mortar-Darcy systems. *Commun. Appl. Math. Comput. Sci.*, **5**, 1–30.

Gander, M. J. (2006) Optimized Schwarz methods. *SIAM J. Numer. Anal.*, **44**, 699–731.

Gander, M. J., Halpern, L. & Magoulès, F. (2007) An optimized Schwarz method with two-sided Robin transmission conditions for the Helmholtz equation. *Int. J. Numer. Meth. Fluids*, **55**, 163–175.

Gander, M. J. & Vanzan, T. (2017) Optimized Schwarz methods for advection diffusion equations in bounded domains. *European Conference on Numerical Mathematics and Advanced Applications*. Springer, pp. 921–929.

Gander, M. J. & Vanzan, T. (2019) Heterogeneous optimized Schwarz methods for second order-elliptic PDEs. *SIAM J. Sci. Comput.*, **41**, A2329–A2354.

Gander, M. J. & Vanzan, T. (2020a) On the derivation of optimized transmission conditions for the Stokes–Darcy coupling. *Domain Decomposition Methods in Science and Engineering XXV. DD 2018, vol. 138 of Lecture Notes in Computational Science and Engineering* (R. Haynes, S. MacLachlan, X.-C. Cai, L. Halpern, H. H. Kim, A. Klawonn, O. Widlund eds). Switzerland: Springer Nature.

Gander, M. J. & Vanzan, T. (2020b) Multilevel optimized Schwarz methods. *SIAM J. Sci. Comput.*, **42**, A3180–A3209.

Gander, M. J. & Xu, Y. (2016) Optimized Schwarz methods for model problems with continuously variable coefficients. *SIAM J. Sci. Comput.*, **38**, A2964–A2986.

Gander, M. J. & Zhang, H. (2019) A class of iterative solvers for the Helmholtz equation: factorizations, sweeping preconditioners, source transfer, single layer potentials, polarized traces, and optimized Schwarz methods. *SIAM Rev.*, **61**, 3–76.

Gigante, G., Sambataro, G. & Vergara, C. (2020) Optimized Schwarz methods for spherical interfaces with application to fluid-structure interaction. *SIAM J. Sci. Comput.*, **42**, A751–A770.

Gigante, G. & Vergara, C. (2016) Optimized Schwarz method for the fluid-structure interaction with cylindrical interfaces. *Domain Decomposition Methods in Science and Engineering XXII*. Cham Heidelberg, New York, Dordrecht, London: Springer, pp. 521–529.

Hairer, E., Lubich, C. & Wanner, G. (2002) *Geometric Numerical Integration: Structure-Preserving Algorithms for Ordinary Differential Equations* Springer series in Computational Mathematics. Berlin, Heidelberg: Springer.

He, X., Li, J., Lin, Y. & Ming, J. (2015) A domain decomposition method for the steady-state Navier–Stokes–Darcy model with Beavers–Joseph interface condition. *SIAM J. Sci. Comput.*, **37**, S264–S290.

JÄGER, W. & MIKELIĆ, A. (1996) On the boundary conditions at the contact interface between a porous medium and a free fluid. *Ann. Scuola Norm. Sup. Pisa Cl. Sci.*, **23**, 403–465.

JOHN, V., MATTHIES, G. & RANG, J. (2006) A comparison of time-discretization/linearization approaches for the incompressible Navier–Stokes equations. *Comput. Methods Appl. Mech. Engrg.*, **195**, 5995–6010.

LACIS, U. & BAGHERI, S. (2017) A framework for computing effective boundary conditions at the interface between free fluid and a porous medium. *J. Fluid Mech.*, **812**, 866–889.

LAGARIAS, J. C., REEDS, J. A., WRIGHT, M. H. & WRIGHT, P. E. (1998) Convergence properties of the Nelder–Mead simplex method in low dimensions. *SIAM J. Optim.*, **9**, 112–147.

LAYTON, W. L., SCHIEWECK, F. & YOTOV, I. (2003) Coupling fluid flow with porous media flow. *SIAM J. Num. Anal.*, **40**, 2195–2218.

LEVY, T. & SANCHEZ-PALENCIA, E. (1975) On the boundary conditions for fluid flow in porous media. *Int. J. Engng. Sci.*, **13**, 923–940.

MARDAL, K. A. & WINTHER, R. (2011) Preconditioning discretizations of systems of partial differential equations. *Numer. Linear Algebr. Appl.*, **18**, 1–40.

MORAITI, M. (2012) On the quasistatic approximation in the Stokes–Darcy model of groundwater-surface water flows. *J. Math. Anal. Appl.*, **394**, 796–808.

RYBAK, I. & MAGIERA, J. (2014) A multiple-time-step technique for coupled free flow and porous medium systems. *J. Comput. Phys.*, **272**, 327–342.

SAAD, Y. & SCHULTZ, M. H. (1986) GMRES: a generalized minimal residual algorithm for solving nonsymmetric linear systems. *SIAM J. Sci. Stat. Comput.*, **7**, 856–869.

SAFFMAN, P. G. (1971) On the boundary condition at the interface of a porous medium. *Stud. Appl. Math.*, **1**, 93–101.

THI-THAO-PHUONG, H., KUNWAR, H. & LEE, H. (2022) Nonconforming time discretization based on Robin transmission conditions for the Stokes–Darcy system. *Appl. Math. Comput.*, **413**, 126602.

TUREK, S. (1996) A comparative study of time-stepping techniques for the incompressible Navier–Stokes equations: from fully implicit non-linear schemes to semi-implicit projection methods. *Int. J. Numer. Meth. Fluids*, **22**, 987–1011.